NATIONAL RESEARCH COUNCIL OF CANADA

AERONAUTICAL REPORT
LR-507

NUMERICAL SOLUTIONS OF THE FLOW FIELD FOR CONICAL BODIES IN A SUPERSONIC STREAM

by

D. J. JONES

NATIONAL AERONAUTICAL ESTABLISHMENT

OTTAWA

JULY 1968

NRC No.

NUMERICAL SOLUTIONS OF THE FLOW FIELD FOR CONICAL BODIES IN A SUPERSONIC STREAM

by

D. J. JONES

W. J. Rainbird, Head
High Speed Aerodynamics Section

F. R. Thurston
Director

SUMMARY

A numerical procedure for solving the problem of steady supersonic inviscid flow around smooth conical bodies is presented. Results are obtained by solving the elliptic partial differential equations that define the conical flow between the body and the shock. Results are given for circular cones up to moderately high relative incidences, including some cases for incidences beyond a critical value at which the entropy singularity moves from the surface.

Also presented are a few results for elliptic cones at zero and non-zero incidence, as well as results for another conical body whose cross section is defined by a fourth order even cosine Fourier series.

The applicability of the method can be limited by the entropy singularity moving too far away from the surface, by the flow field containing regions of locally conically supersonic flow, or by the shock wave approaching very close to the Mach wave.

Comparison of results shows excellent agreement with other theoretical methods and also with experimental results. The method is efficient in computer time.

CONTENTS

TABLES

ILLUSTRATIONS

ILLUSTRATIONS (Cont'd)

APPENDICES

SYMBOLS

Symbol	Definition
A,B,C,A′,B′,C′	Square matrices (5 × 5), see equation (1)
a,b	Semi-major and semi-minor axes of an elliptic cone at unit distance from the cone apex
c	Local speed of sound
c_{cr}	Critical speed of sound
D,D′	Vectors, see equation (1)
d	$\equiv v - Gu - \frac{G_\phi}{G} w$
f	$r = f(z, \theta)$ defines the equation of a shock wave
F	$r = z F(\theta)$ defines the equation of the conical shock wave
$F_0,F_1,F_2 \ldots$	Constant coefficients of the Fourier series used to define the shock shape
g	$r = g(z,\theta)$ defines a general body
G	$r = z G(\theta)$ defines the equation of the conical body
$G_{\phi\phi}$	Second derivative of G with respect to ϕ
G_0,G_2,G_4	Constant coefficients used to define a body shape given by a fourth order even cosine Fourier series
h	Static enthalpy
M	Local Mach number
M_c	Surface Mach number
p	Pressure
$\bar{p}$	Pressure non-dimensionalised with respect to $\rho_\infty c_{cr}^2$
$p_{\phi\phi}$	Second derivative of p with respect to ϕ
p_c	Surface pressure
r	Radial distance from the z-axis

SYMBOLS (Cont'd)

Symbol	Definition
S	An entropy function defined as $\log \frac{p}{\rho^{\gamma}}$, $(\log \frac{p_{\infty}}{\rho_{\infty}^{\gamma}} = 0)$
(u, v, w)	Velocity components in the (z,r,θ) directions, respectively
$(\bar{u}, \bar{v}, \bar{w})$	(u, v, w) non-dimensionalised with respect to c_{cr}.
V_{∞}	Free stream velocity
V_{n_c}	Normal velocity at the cone surface
(x, ξ, ϕ)	A co-ordinate system obtained by transformation of the system (z, r, θ)
X	A vector, see equation (1)
(z, r, θ)	A cylindrical co-ordinate system (see Fig. 1) with z along the cone axis
α	Angle of incidence
γ	Ratio of specific heats C_p/C_v, taken as 1.4 for the present computations
$\delta\xi$	A small increment in the independent variable ξ
$\delta\phi$	A small increment in the circumferential angle ϕ
ϵ_2, ϵ_4	Small changes made to G_2, G_4
θ	Circumferential angle, $\theta = 0$ on the windward side and $\theta = \pi$ on the leeward side
θ_c	Semi-apex angle of circular cone
ξ	An axis of the transformed co-ordinate system $\xi = \frac{r - z\,G(\theta)}{z[F(\theta) - G(\theta)]}$
ρ	Density
$\bar{\rho}$	Density non-dimensionalised with respect to ρ_{∞}
ϕ	Transformed circumferential angle, $\phi \equiv \theta$
Subscripts	
∞	Free stream values
c	At the conical surface

SYMBOLS (Cont'd)

Symbol	Definition
Subscripts	
s	At the shock surface (downstream)
n	Normal component
n_c	Normal component at the conical surface
z, r, θ, x, ξ, ϕ	Partial differential with respect to these variables

1.0 INTRODUCTION

The first attempts to obtain solutions for the steady inviscid supersonic flow field about conical bodies were made by several authors in the early 1930's. These authors considered a circular cone at zero incidence to the free stream. The equations defining the flow were reduced to ordinary non-linear differential equations to be satisfied between the shock and the body, thus giving a two-point boundary value problem. These equations were numerically integrated by Kopal in 1947 (Ref. 1) using the equations as derived by Taylor and Macoll in 1932. Later, Sims computed these zero order solutions again and presented the results in a convenient form in Reference 2.

Using a small perturbation method, Stone in 1948 (Ref. 3) produced a first order solution applicable to circular cones at small incidence. Kopal made the original numerical integration of the resulting equations, and Sims (Ref. 4) later repeated and extended the calculations. A second order theory for a circular cone was also formulated by Stone (Ref. 5), and Kopal in 1949 again provided numerical results. These second order tabulations of Kopal (Ref. 6) are of limited range and inconvenient to use.

These first and second order solutions contain uncertainties, as pointed out by Ferri (Ref. 7), owing to the singularity in entropy not being included. Ferri observed that the body must be a surface of constant entropy and that all streamlines must eventually converge at the leeward generator of the cone, thus resulting in an entropy singularity at this line. Ferri also pointed out that there is a layer very close to the surface, the vortical layer, in which the entropy changes rapidly in a direction normal to the surface.

Melnik, amongst others, studied in detail the vortical layer and the position of the entropy singularities (Ref. 8 and 9) for a circular cone and a delta wing and was able to show that, in the case of the circular cone, the nodal type singularity remained at the leeward generator until an incidence was reached when the transverse pressure gradient became adverse. Beyond this incidence it was shown that the nodal singularity might follow the point of minimum pressure or might stay at the leeward generator until a certain incidence was reached, at which time the singularity would lift off the cone surface. It is shown in this Report that the latter is the correct behaviour.

Several numerical techniques have been developed in recent years to solve the problem, particularly for cones that are circular or elliptical in cross section. Stocker and Mauger (Ref. 10), amongst others, solved the set of elliptic partial differential equations that apply between the shock wave and the body, assuming a shock shape and integrating in towards a body that is defined by the envelope of the streamlines obtained in the integration procedure. The shock shape was then modified empirically to obtain a given body shape. Results were presented for the circular cone with a semi-apex angle of 20° (at incidences of 5° and 10°) for a Mach number of 3.53. The results for the 5° incidence agree well with experiment, while only fair agreement was obtained at 10° incidence. In fact, difficulties were encountered in the iteration procedure for the 10° incidence case and it was not possible to obtain a solution for an incidence of 15°. At this larger incidence, the computed body seemed to have a "bump" located at and near the leeward generator, which at that time was thought to be accounted for by the singularity leaving the body. Stocker and Mauger's method can also, in principle, be applied to other bodies besides circular cones, and a computation was made for an elliptic cone at zero incidence, the results of which gave reasonable agreement with experiment.

A different numerical method of solving the problem for any conical body was proposed by Babenko et al. (Ref. 11). In this method the full three-dimensional flow field equations are considered and, starting from an estimated shock shape with the given body set at the required incidence, the equations are integrated step by step downstream until a condition of conicity is reached. When this condition is reached, the full flow field solution is then available.

Reference 11 gives tabulated values of the flow field quantities for circular cones at incidence. Some results are given for Mach numbers of 2, 3, 4, 5, 6, and 7, cone semi-angles of from 10° to 45° in 5° steps, and for relative incidences up to 0.8. Most of the Mach number 4 and 6 results were obtained by interpolation from the results at the other Mach numbers. These numerical results show excellent agreement with experiment.

Gonidou (Ref. 12) has used the method of Babenko et al. to obtain solutions for a circular cone at relative incidence, α/θ_c, up to about 1.2 where the entropy singularity has lifted from the surface of the cone at the leeward generator. Solutions for elliptic cones of fairly high eccentricity ($\sim$3) were also obtained by Gonidou. Computer times and some other program details for the Babenko method are given in his paper. About 500 downstream steps are required to reach a condition of conicity, and about ½ hour is required for a typical solution on a CDC 3600 computer for a mesh size of 10 x 16 in the radial and circumferential directions respectively.

Moretti (Ref. 13) has used a similar approach to that of Babenko et al. Again, the flow field solution is obtained by marching step by step downstream until a conicity condition is sufficiently well satisfied. The method differs from Babenko's method in the details of numerical analysis and in his use of a characteristics method on the shock and on the body. Moretti's method requires about 400 downstream steps and the computer time is typically ½ hour on an IBM 360/50 computer. This time is applicable to a mesh increment that is about twice the size of that used by Gonidou in the time quoted above. To get a true comparison of computer times, it should be noted that a CDC 3600 computer operates at about twice the speed of an IBM 360/50 computer.

The purpose of investigating a further numerical technique, as given in this Report, was not only to try to find a more efficient technique than those given previously, but also to investigate a method that, in principle, is capable of solving non-linear elliptic partial differential equations; in itself a difficult problem in numerical analysis. The present method uses the condition of conicity to reduce the problem to a set of elliptic non-linear partial differential equations in two independent variables. A transformation of co-ordinates is used, as in the methods of Babenko and Moretti, to fix the boundaries between which the elliptic equations are to be satisfied. This transformation also has the effect of including the body shape in the coefficients of the partial differential equations and in the boundary conditions, so that the same method can be used for general conical body shapes simply by changing a few program statements to redefine the equation of the body. In fact, the method is, in most cases, only limited by locally supersonic cross-flow conditions, or by the entropy singularity moving too far away from the surface, or by the shock approaching very close to the Mach wave.

At the present time the method has been used successfully for circular cones and for bodies that can be obtained by successive perturbations of a circular cone and that do not have curvatures that are too large. The examples given here are for circular cones at incidence, elliptic cones, and a body whose cross-sectional shape is represented by a fourth order even cosine Fourier series.

The method is efficient in computer time compared with other fully numerical techniques and one solution takes from about ½ minute to 3 minutes on an IBM 360/50 computer for the circular cone at incidence — the time increasing as the incidence increases.

2.0 EQUATIONS OF MOTION AND THE BOUNDARY CONDITIONS

2.1 The Equations of Motion and the Boundary Conditions for a General Body

The co-ordinate system and equations of motion are written in a notation similar to that used in Reference 11.

Let (z, r, θ) be a cylindrical co-ordinate system as shown in Figure 1. Then the equations of continuity, momentum, and energy for an inviscid, non-heat conducting gas can be written in matrix form in this co-ordinate system as follows

$$A' \frac{\partial X}{\partial z} + B' \frac{\partial X}{\partial r} + C' \frac{\partial X}{\partial \theta} + D' = 0 \tag{1}$$

where

$$A' = \begin{bmatrix} u & 0 & 0 & 1/\rho & 0 \\ 0 & u & 0 & 0 & 0 \\ 0 & 0 & u & 0 & 0 \\ \rho c^2 & 0 & 0 & u & 0 \\ \rho & 0 & 0 & 0 & u \end{bmatrix}$$

$$B' = \begin{bmatrix} v & 0 & 0 & 0 & 0 \\ 0 & v & 0 & 1/\rho & 0 \\ 0 & 0 & v & 0 & 0 \\ 0 & \rho c^2 & 0 & v & 0 \\ 0 & \rho & 0 & 0 & v \end{bmatrix}$$

$$C' = \frac{1}{r} \begin{bmatrix} w & 0 & 0 & 0 & 0 \\ 0 & w & 0 & 0 & 0 \\ 0 & 0 & w & 1/\rho & 0 \\ 0 & 0 & \rho c^2 & w & 0 \\ 0 & 0 & \rho & 0 & w \end{bmatrix}$$

$$D' = \frac{1}{r} \begin{bmatrix} 0 \\ -w^2 \\ wv \\ \rho c^2 v \\ \rho v \end{bmatrix} \quad \text{and} \quad X = \begin{bmatrix} u \\ v \\ w \\ p \\ \rho \end{bmatrix}$$

In the above matrices and vectors (u, v, w) are the velocity components in the (z, r, θ) directions respectively, p is the pressure, ρ the density, and c^2 the square of the local speed of sound.

Boundary conditions are given at the body and at the shock. The boundary condition on the body is that the normal velocity should be zero. Thus, if the equation of the body is $r = g(z, \theta)$ then the boundary condition on this body is

$$u \frac{\partial g}{\partial z} - v + \frac{w}{g} \frac{\partial g}{\partial \theta} = 0 \tag{2}$$

Velocity components, pressure, and density behind the unknown shock can be found in terms of the shock equation by applying the Rankine-Hugoniot relations across the discontinuity, giving the following equations

$$\begin{aligned}
\rho V_n &= \rho_\infty V_{n\infty} \\
p + \rho_\infty V_{n\infty} V_n &= p_\infty + \rho_\infty V_{n\infty}^2 \\
h + \tfrac{1}{2} V_n^2 &= h_\infty + \tfrac{1}{2} V_{n\infty}^2 \\
u + v \frac{\partial f}{\partial z} &= u_\infty + v_\infty \frac{\partial f}{\partial z} \\
\frac{v}{f} \frac{\partial f}{\partial \theta} + w &= \frac{v_\infty}{f} \frac{\partial f}{\partial \theta} + w_\infty
\end{aligned} \tag{3}$$

where V_n is the velocity component normal to and behind the shock, and is given by

$$V_n = \frac{u \frac{\partial f}{\partial z} - v + \frac{w}{f} \frac{\partial f}{\partial \theta}}{\sqrt{1 + \left(\frac{\partial f}{\partial z}\right)^2 + \left(\frac{1}{f} \frac{\partial f}{\partial \theta}\right)^2}}$$

h is the static enthalpy ($\equiv \frac{\gamma}{\gamma-1} \frac{p}{\rho}$ for a calorically perfect gas) and the equation of the shock is given by $r = f(z, \theta)$. The subscript ∞ refers to values in front of the shock wave, hence

$$u_\infty = V_\infty \cos \alpha, \; v_\infty = - V_\infty \sin \alpha \cos \theta, \; w_\infty = V_\infty \sin \alpha \sin \theta$$

and

$$V_{n\infty} = \frac{u_\infty \frac{\partial f}{\partial z} - v_\infty + \frac{w_\infty}{f} \frac{\partial f}{\partial \theta}}{\sqrt{1 + \left(\frac{\partial f}{\partial z}\right)^2 + \left(\frac{1}{f} \frac{\partial f}{\partial \theta}\right)^2}}$$

where V_∞ is the free stream velocity.

The present Report deals with situations that are conical, hence the number of independent variables can be reduced from three to two. A suitable transformation to carry out this reduction is made in the following paragraph.

2.2 Transformation of the Independent Variables

The equations given in the previous paragraph apply to any general body shape $r = g(z, \theta)$ and a shock wave given by $r = f(z, \theta)$. However, we now consider a situation in which the body and flow characteristics are conical so that the number of independent variables can be reduced from three to two.

Firstly it is seen that, since the z-axis is along the axis of the cone with the origin at the apex, the equation of the conical body can be written

$$r = z\, G(\theta)$$

where $G(\theta)$ is a function of θ only, and similarly the equation of the conical shock wave can be written

$$r = z\, F(\theta)$$

where $F(\theta)$ is a function of θ only.

Now the independent variables (z, r, θ) are transformed by transformations involving the equations of the body and the shock as follows

$$x = z$$

$$\xi = \frac{r - z\, G\ (\theta)}{z\, [\, F\ (\theta) - G\ (\theta)\ ]}$$

$$\phi = \theta$$

This transformation has the effect of fixing the radial as well as the circumferential boundaries between which the partial differential equations are to be satisfied, since now the body $r = z\, G(\theta)$ corresponds to the surface $\xi = 0$, while the shock $r = z\, F(\theta)$ corresponds to the surface $\xi = 1$.

The above transformations change the equations of motion (1) to the form

$$A \frac{\partial X}{\partial x} + B \frac{\partial X}{\partial \xi} + C \frac{\partial X}{\partial \phi} + D = 0$$

where

$$A = A'$$

$$B = \xi_z\, A' + \xi_r\, B' + \xi_\theta\, C'$$

$$C = C'$$

$$D = D'$$

and the subscripts denote partial differentiation so that ξ_z, ξ_r, and ξ_θ can be evaluated as

$$\xi_r = \frac{1}{z\ (F - G)}$$

$$\xi_z = - \xi_r\, [G + (F - G)\xi] \qquad (4)$$

$$\xi_\theta = - z\, \xi_r\, [G_\theta + (F_\theta - G_\theta)\, \xi]$$

In the new co-ordinate system (x, ξ, ϕ) the region in which the equations are to be satisfied is

$$x > 0$$

$$0 \leq \xi \leq 1$$

$$0 \leq \phi \leq 2\, \pi$$

However, since the flow is conical, quantities are constant for all x and for a fixed ξ and ϕ, thus $\frac{\partial X}{\partial x} = 0$. The problem is then reduced to two dimensions in the independent variables ξ and ϕ and we may consider the equations at a unit distance ($x = z = 1$) along the body.

Thus the problem is reduced to that of solving the elliptic non-linear partial differential equations

$$B\frac{\partial X}{\partial \xi} + C\frac{\partial X}{\partial \phi} + D = 0 \tag{5}$$

subject to the boundary conditions given in the next paragraph.

2.3 The Boundary Conditions for a Conical Body

In the transformed co-ordinate system the boundary conditions become, from equation (2), at $\xi = 0$

$$u\,G - v + \frac{w}{G}\frac{\partial G}{\partial \phi} = 0 \tag{6}$$

and at $\xi = 1$, from equations (3)

$$\begin{aligned}
&\rho V_n = \rho_\infty V_{n\infty} \\
&p + \rho_\infty V_{n\infty} V_n = p_\infty + \rho_\infty V_{n\infty}^2 \\
&h + \tfrac{1}{2} V_n^2 = h_\infty + \tfrac{1}{2} V_{n\infty}^2 \\
&u + v\,F = u_\infty + v_\infty F \\
&\frac{v}{F}\frac{\partial F}{\partial \phi} + w = \frac{v_\infty}{F}\frac{\partial F}{\partial \phi} + w_\infty
\end{aligned} \tag{7}$$

where

$$V_n = \frac{u\,F - v + \dfrac{w}{F}\dfrac{\partial F}{\partial \phi}}{\sqrt{1 + F^2 + \left(\dfrac{1}{F}\dfrac{\partial F}{\partial \phi}\right)^2}}$$

and the equations of the body and shock have transformed to

$$r = G(\phi)$$

and

$$r = F(\phi)$$

respectively.

Further boundary conditions can be applied if the body and flow characteristics are symmetrical about the axis $\theta(\equiv \phi) = 0, \pi$ as is often the case. In this case boundary conditions at $\phi = 0, \pi$ are

$$\frac{\partial u}{\partial \phi} = \frac{\partial v}{\partial \phi} = \frac{\partial p}{\partial \phi} = \frac{\partial \rho}{\partial \phi} = w = 0$$

and the problem is reduced to solving the equations in the region

$$0 \le \xi \le 1$$

$$0 \le \phi \le \pi$$

In the next Section a summary of the method for solving the set (5), subject to the given boundary conditions, is presented; a more detailed description is presented in Appendix A.

3.0 METHOD OF SOLUTION

We observe that if the function $F(\phi)$ defining the shock shape is known, the problem is solved completely, since then the equations (7) can be solved to give u, v, w, p, ρ at $\xi = 1$ and equations (5) can be integrated from $\xi = 1$ to $\xi = 0$ by replacing the elements of $\frac{\partial X}{\partial \phi}$ by difference formulae of the type (A-1) (see Appendix A). This makes the set (5) into ordinary differential equations and they can be integrated by standard techniques such as those given in Reference 14. However, $F(\phi)$ is not known initially, but it is assumed that we have a reasonable estimate so that the equations (5) can be integrated as above. Using the estimated $F(\phi)$ then, after integration, a "residual" normal velocity given by the value of the left-hand side of equation (6) at $\xi = 0$ will be obtained. The problem then is to minimise the residual at $\xi = 0$, for all ϕ, by changing the function $F(\phi)$. This minimisation is carried out by the iteration procedure described in Appendix A.

In the method described in Appendix A it is necessary for the conical flow solutions required here to have a good initial estimate of $F(\phi)$, so that the integration will not diverge. To obtain a good estimate of the shock shape $F(\phi)$ for conical bodies, the following procedure is adopted. The flow field solution is first found for a circular cone at zero incidence by means of the iteration procedure described in Appendix D. A very small perturbation is then made in either body shape or incidence (for example an elliptic cone of small eccentricity or a circular cone at very small incidence is considered) and for this situation a solution is sought, using for the initial estimate of $F(\phi)$ the value obtained for the circular cone at zero incidence. Having obtained the solution for the small perturbation, a much bigger perturbation of the same type is made and the function $F(\phi)$ extrapolated so that a good initial estimate is still available. For example, in the case of a circular cone at incidence, a solution is first found for an incidence α where $\alpha/\theta_c = 0.01$, then $F(\phi)$ is extrapolated linearly to $\alpha/\theta_c = \delta\alpha$ where $\delta\alpha \simeq 0.1$ to give an initial estimate, and the final solution at that incidence is found by iteration as mentioned above. After this computation a quadratic extrapolation of $F(\phi)$ is made to give an initial estimate at $\alpha/\theta_c = 2\,\delta\alpha$ and so on to higher incidences.

In the case of the circular cone at incidence, the function $F(\phi)$ is represented adequately by a Fourier series

$$F(\phi) = \sum_{i=0}^{m} F_i \cos i\phi \tag{8}$$

since $F(\phi)$ must be symmetrical about $\phi = 0$ and $\phi = \pi$ ($\phi = 0$ is the windward plane of symmetry and $\phi = \pi$ is the leeward plane of symmetry). This form has the advantage that m can be kept small ($= 1$ or 2) for small incidences, thus giving fewer "unknowns" to the problem and economising on the iteration process to determine $F(\phi)$. The value of m, however, must be increased as the incidence is increased. Now as m increases, the representation (8) of the function $F(\phi)$ may still be good, but the derivative of the Fourier series may not be a good representation of $\frac{\partial F}{\partial \phi}$, so instead of obtaining $\frac{\partial F}{\partial \phi}$ by differentiation of (8) the difference formula (A-1) is used.

A difficulty that must be overcome in integrating the ordinary differential equations that represent the set (5) is that some of the derivatives $\frac{\partial}{\partial \xi}$ are not defined at $\xi = 0$. This is observed by examining the equations at $\xi = 0$ where we have

$$\xi_r \, d \, u_\xi - \frac{\xi_r G}{\rho} \, p_\xi + \frac{w}{G} \, u_\theta = 0 \qquad (a)$$

$$\xi_r \, d \, v_\xi + \frac{\xi_r}{\rho} \, p_\xi + \frac{w}{G} \, v_\theta = \frac{w^2}{G} \qquad (b)$$

$$\xi_r \, d \, w_\xi - \frac{\xi_r \, G_\theta}{\rho G} \, p_\xi + \frac{w}{G} \, w_\theta + \frac{p_\theta}{\rho G} = - \frac{wv}{G} \qquad (c) \qquad (9)$$

$$\xi_z \, \rho c^2 \, u_\xi + \xi_r \, \rho c^2 \, v_\xi + \frac{\xi_\theta \, \rho c^2}{r} w_\xi + d' \, p_\xi + \frac{\rho c^2}{r} \, w_\phi + \frac{w}{r} \, p_\phi = - \frac{\rho c^2 \, v}{r} \qquad (d)$$

$$\xi_z \, \rho \, u_\xi + \xi_r \, \rho \, v_\xi + \frac{\xi_\theta \rho}{r} w_\xi + d' \, \rho_\xi + \frac{\rho}{r} \, w_\phi + \frac{w}{r} \, \rho_\phi = - \frac{\rho v}{r} \qquad (e)$$

where $d = v - G \, u - \frac{w}{G} \frac{\partial G}{\partial \phi}$, $d' = \xi_z \, u + \xi_r \, v + \frac{\xi_\theta}{r} w$, and the subscripts z, r, θ, ξ and ϕ refer to partial differentiation with respect to these variables.

It is convenient to rewrite (9d) and (9e) in terms of

$$\frac{\partial}{\partial \xi} \left(\xi_z \, u + \xi_r \, v + \frac{\xi_\theta}{r} \, w \right) \qquad (10)$$

where ξ_z, ξ_r, and ξ_θ are given by equation (4) with $z = 1$. Equations (9d) and (9e) were written above without the limit of $\xi = 0$, thus considering the derivative (10) in connection with (9d) and (9e) is permissible.

Now (10) can be written

$$\xi_z \, u_\xi + \xi_r \, v_\xi + \frac{\xi_\theta}{r} \, w_\xi - u - \frac{w}{r} \left(\frac{F_\phi - G_\phi}{F - G} \right) - \frac{\xi_\theta}{r^2} \, w \, (F - G)$$

and (9d) and (9e) as

$$\rho c^2 \left[\frac{\partial}{\partial \xi} \left(\xi_z \, u + \xi_r \, v + \frac{\xi_\theta}{r} \, w \right) + u + \frac{w}{G} \left(\frac{F_\phi - G_\phi}{F - G} \right) + \frac{\xi_\theta}{G^2} \, w \, (F - G) \right]$$

$$+ \xi_r \, d \, p_\xi + \frac{\rho c^2}{G} \, w_\phi + \frac{w}{G} \, p_\phi = - \frac{\rho c^2 \, v}{G} \qquad (9d')$$

$$\rho \left[\frac{\partial}{\partial \xi} \left(\xi_z \, u + \xi_r + \frac{\xi_\theta}{r} \, w \right) + u + \frac{w}{G} \left(\frac{F_\phi - G_\phi}{F - G} \right) + \frac{\xi_\theta}{G^2} \, w \, (F - G) \right]$$

$$+ \xi_r \, d \, \rho_\xi + \frac{\rho w_\phi}{G} + \frac{w \rho_\phi}{G} = - \frac{\rho v}{G} \qquad (9e')$$

on applying the limit $\xi = 0$.

The boundary condition at the surface (eq. (6)) implies that d = 0 at $\xi = 0$ and hence it is not possible to determine u_ξ, v_ξ, w_ξ, or ρ_ξ at $\xi = 0$ from the surface equations (9). However, if we assume that du_ξ, dv_ξ, dw_ξ, dp_ξ, and $d\rho_\xi$ all tend to zero as $\xi \to 0$, which appears reasonable, and also assume that derivatives of quantities with respect to ϕ are finite on the surface (which is reasonable since the surface is a streamline), then we can at least say that p_ξ is finite from (9a), (9b), or (9c), and that $\frac{\partial}{\partial \xi}\left(\xi_z u + \xi_r v + \frac{\xi_\theta}{r} w\right)$ from (9d′) or (9e′) is also finite at $\xi = 0$.

The previous analysis shows that integration of the differential equations right up to $\xi = 0$ cannot be made by the usual techniques, since these would require calculation of all derivatives with respect to ξ at $\xi = 0$. However, integration can be made to a value $\delta\xi$ close to the surface and the variable $\xi_z u + \xi_r v + \frac{\xi_\theta}{r} w$ can be extrapolated from its value and derivative at points near to the surface (at $\delta\xi$, 2 $\delta\xi$, 3 $\delta\xi$, and 4 $\delta\xi$, for example). Extrapolation of this quantity is permitted, since we have shown its derivative is at least finite at $\xi = 0$. Now the quantity $\left[\xi_z u + \xi_r v + \frac{\xi_\theta}{r} w\right]_{\xi = 0}$ is the normal velocity V_{n_e} at the surface, which we are trying to make zero by the iteration procedure. Thus the problem is solvable by the technique mentioned.

Having completed the iteration to make normal velocity V_{n_e} sufficiently small, a final integration of the set (5) is made to a value of ξ fairly close to the surface (approximately 0.003) and then pressure is obtained at the surface $\xi = 0$ by inward extrapolation from 0.003. Again this extrapolation is permitted since the derivative of p is finite at the surface. The values of V_{n_e} and p thus obtained at the surface allow a complete calculation of the other flow variables at the surface, as follows.

Since the body is a streamline we have

$$\left(\frac{p}{\rho^\gamma}\right)_e = \text{constant} \tag{11}$$

and the constant is equal to the value at a saddle point or points of attachment on the surface — which for the circular cone at incidence is at the windward axis $\phi = 0$ since this axis also forms the same streamline, as pointed out in Reference 7.

Also in the flow field, and hence on the surface for isoenergetic flow

$$\tfrac{1}{2}(u^2 + v^2 + w^2) + \frac{\gamma}{\gamma - 1}\frac{p}{\rho} = \text{constant} \tag{12}$$

where the constant is determined from free steam conditions.

A further condition follows by eliminating p_ξ from (9a) and (9b) (with d = 0)

$$w u_\phi + w G v_\phi = w^2 G \tag{13}$$

The equations (11), (12), (13), together with the boundary condition (6) and the knowledge of the pressure, give five equations to be solved for u, v, w, p, and ρ at the surface. A method of solving these equations for the circular cone at incidence is given in Appendix B. The same method can be used for other conical bodies, provided the positions of the saddle points of attachment on the surface are first determined.

It should be noted that a complete surface solution may not always be necessary since the pressure is found correctly by extrapolation, and it is probably better to use extrapolated or near the surface values of other quantities for, say, boundary-layer calculations. This follows from the assumption that the vortical layer (the layer near the surface where large gradients are present) is much thinner than the boundary layer.

4.0 A SHORT DISCUSSION OF THE VORTICAL LAYER

It has been pointed out (Ref. 7, 8, and 9) that in non-axisymmetric conical supersonic flow, large gradients in some quantities are present very near to the surface. It was shown in Section 3.0 by examining the equations of motion on the surface, that the derivatives of pressure p and normal velocity $\xi_z u + \xi_r v + \frac{\xi_\theta}{r} w$ were finite at the surface, while derivatives of other quantities were indeterminate. Since only the normal velocity at the surface was required for iteration and the pressure p was required to solve the surface equations completely, the present method overcame any difficulties due to large gradients within the vortical layer. For completeness, however, an integration of the set (5) was performed, taking very small increments in ξ as the surface was approached. Figure 2 shows plots of the velocity components $\bar{u}$ and $\bar{w}$ and the density profile near to the surface for the particular case of a circular cone with $M_\infty = 7$, $\theta_c = 25$, $\alpha = 10$ at $\phi = 90°$.

Also, for completeness, Table 1 shows a comparison between surface values of pressure obtained by integration near to the surface and those obtained in the usual method of this Report (i.e. by inward extrapolation from $\xi \approx 0.003$). The tabulated results are for the case $M_\infty = 1.797$, $\theta_c = 12.5°$, $\alpha = 7.5°$; this example is chosen since there is a fairly noticeable change in pressure near to the surface (for the above case of $M_\infty = 7$, $\theta_c = 25$, $\alpha = 10°$ there is very little change in pressure). The adequacy of the usual method of extrapolation is well illustrated.

5.0 COMPARISON OF THE PRESENT RESULTS WITH THOSE OF OTHER THEORETICAL METHODS FOR THE CIRCULAR CONE AT INCIDENCE

Figures 3, 4, and 5 show comparisons of the present theory with the results of first order theory given in Reference 4. Figure 4 also shows a comparison with the results of Moretti (Ref. 13), while Tables 2 to 9 give comparisons of the present theory with that due to Babenko et al. (Ref. 11).

It can be seen from these Tables that almost exact agreement is obtained between the present results and those of Reference 11, while the results of Reference 13 differ by a larger amount, probably because of the differences in step size used.

The step sizes used by Babenko were $\delta\xi = 0.05$ and $\delta\phi = 11.25°$, by Moretti $\delta\xi = 0.167$ and $\delta\phi = 18°$, and with the present method $\delta\xi = 0.1$ and $\delta\phi = 22\frac{1}{2}°$ for most of the cases in which comparisons were made in this Report. Good accuracy is obtained with the present method even though larger step sizes are used. This is to be expected since the errors are $0\ (\delta\phi^4)$ and $0\ (\delta\xi^5)$ in the present scheme.

The first order results agree, as expected, for small relative incidences only, and the inadequacy of the first order theory is noted even for relative incidences of about 0.5. Results from References 11 and 13 are available only for relative incidences α/θ_c up to about 0.8. At present, accurate tabulated results for higher relative incidences are not available, so that comparisons cannot be made with other theoretical methods for relative incidences higher than 0.8. However, a comparison with experimental results is made in the next Section, which extends to higher relative incidences.

6.0 COMPARISON OF PRESENT RESULTS WITH EXPERIMENT FOR THE CIRCULAR CONE

Experiments to measure surface pressures on 12.5° and 5° circular cones have been made at NAE under high Reynolds' number conditions (Ref. 15 and 16). The experiments were conducted over a wide range of Mach numbers from 1.8 to 4.25 and with relative incidences from zero to about 2.5. Figures 6 — 9 show a comparison of surface pressure ratio p/p_∞ as calculated by the present method with the experimental data.

In most cases the greatest difference between the theory and experiment occurs in the region $\phi = 0°$ to 30°. It is known that the high surface shear stress in this region leads to appreciable positive hole errors in the measured static pressures (Ref. 17), but the exact magnitude is difficult to estimate in each case.

It can be seen from the Figures that excellent agreement is obtained in the region from $\phi = 30°$ to 180°, even at incidences where the singularity has left the surface, e.g. $M_\infty = 1.8$, $\theta_c = 12.5°$, $\alpha = 17.5°$, and also where locally conically supersonic conditions are just becoming present near the surface, e.g. $M_\infty = 4.25$, $\theta_c = 12.5°$, $\alpha = 12.5°$. The present method is limited to incidences below some critical value at which a region of the flow becomes locally conically supersonic, However, it can be seen that surface pressures extrapolated from incidences below this critical incidence (by quadratic extrapolation) still give good agreement with the experiment, at least in the region of the flow where separation does not have large effect (see, for example, Fig. 10).

7.0 THE ELLIPTIC CONE IN SUPERSONIC FLOW

Most of the discussions in this Report have been concerned with circular cones at incidence. However, the method of solution is applicable, at least in principle, to any conical body with conically subsonic flow. As a further example of the method some calculations were made for elliptic cones at zero incidence, and at incidence but without yaw, again starting from the $\alpha = 0$ circular cone solution. Some of these results (the surface pressures) are compared with another theoretical method (Ref. 18) and with experiments (Ref. 19) in Figures 11 and 12. It can be seen from these Figures that the present method gives much better agreement with the experiments, particularly for the cases at incidence, than the linearised characteristics solutions of Martellucci (Ref. 18).

The method has been found to be less efficient when the ratio of major to minor axes, a/b, becomes so high that large gradients in quantities occur in the flow field near the "leading edge". Very small increments $\delta\phi$ are needed for the difference scheme (A-1). A reasonable limit for the ratio a/b seems to be within the range 2 to 3, (see computer times, App. E.4.2).

8.0 A FURTHER EXAMPLE OF A CONICAL BODY IN SUPERSONIC FLOW

As a further example to illustrate the use of the present method, computations were made for the conical body given by

$$r = G_0 + G_2 \cos 2\phi + G_4 \cos 4\phi$$

at a unit distance $z = 1$ from the body tip, where G_0, G_2, and G_4 are constants (0.2679, −0.01, and 0.02 respectively, in the example for which results are given). The computation was started from a circular cone at zero incidence ($G_2 = G_4 = 0$) and G_2 and G_4 were given small values (ϵ_2, ϵ_4, say)

and a solution obtained. G_2 and G_4 were then increased proportionally to ϵ_2 and ϵ_4 and an initial estimate of the shock shape was made by extrapolation from the solution with $G_2 = \epsilon_2$ and $G_4 = \epsilon_4$, and a solution was again obtained by iteration. G_2 and G_4 were increased again proportionally to ϵ_2 and ϵ_4 and the process continued.

Figure 13 shows the shock shape and the surface pressure distribution corresponding to $G_0 = 0.2679$, $G_2 = -0.01$, $G_4 = 0.02$ at zero incidence. Figure 14 shows pressure distributions and also indicates the circumferential angles at which nodal and saddle type singular points on the surface are present for the same body at several incidences.

This example illustrates well the singularity behaviour to be expected for this type of indented body. It can be seen that at zero incidence there are two nodal and three saddle type singular points on the surface in the range $0 \leq \phi \leq 180$. As the incidence is increased the nodal and one of the saddle type singularities on the windward side combine to "cancel" each other so that the surface streamlines now converge only near to the leeward generator. As the incidence is further increased the nodal type singularity near to the leeward generator moves around to eventually lie on the leeward generator where previously there was a saddle type singular point. The positions of the singularities are easily determined from the direction of the streamlines as integration is made into the surface, and it is also known that they can be located at points on the surface only where the circumferential gradient of pressure is zero.

9.0 CONCLUSIONS

A method has been presented that shows that the elliptic partial differential equations defining the conical inviscid flow between a conical body and its conical shock wave are solved very efficiently by a numerical approach.

A transformation is used that has the effect of including the body shape in the coefficients of the differential equations and of the boundary conditions, thus making the computer program suitable, in principle, for any conical situation simply by writing a few program statements to define the body shape.

Solutions have been obtained by making successive perturbations to a circular cone at zero incidence for which the flow field solution is readily available. Perturbations of incidence were made to obtain results for circular cones at incidence and have given good results even at relative incidences higher than any other known fully numerical method. To generate solutions for an elliptic cone, perturbations were made first in body shape and then in incidence, if solutions at incidence were required. Similarly, solutions can be obtained for other conical body shapes, such as those obtained for the body given by a fourth order even cosine Fourier series.

It was shown that excellent agreement with other theoretical methods (in particular that due to Babenko et al. (Ref. 11) for the circular cone) and also with experiment, was obtained. At the same time, solutions were generated at about 30 to 50 times faster with the present method (typical computer times are quoted in App. E.4.0) than with other fully numerical, accurate techniques.

At present the method appears to be limited to cases that do not have regions of conically supersonic flow, since, if such regions do exist, the defining equations in these regions become hyperbolic while they remain elliptic in the other regions. Two other conditions also present a limit to the applicability of the method. These occur when an entropy singularity moves sufficiently far away from the surface that it lies very near to the first exterior set of mesh points, and also when the shock wave approaches very close to the Mach cone from the apex, which occurs for very slender conical flows at low supersonic Mach numbers.

10.0 ACKNOWLEDGEMENTS

The author wishes to thank W. J. Rainbird and R. F. Meyer for useful discussions held during the course of this project. He is also grateful to G. Moretti of General Applied Science Laboratory, New York, for supplying the computer program to carry out the computations described in Reference 13.

11.0 REFERENCES

1. Kopal, Z. — Tables of Supersonic Flow Around Cones. Massachusetts Institute of Technology, Dept. of Electrical Engineering Tech. Report No. 1, Cambridge, Mass., 1947.

2. Sims, J. L. — Tables for Supersonic Flow Around Right Circular Cones at Zero Angle of Attack. NASA SP-3004, National Aeronautics and Space Administration, Washington, 1964.

3. Stone, A. H. — On the Supersonic Flow Past a Slightly Yawing Cone, Part I. Journal of Mathematics and Physics, Vol. 27, No. 1, April 1948, pp. 67-81.

4. Sims, J. L. — Tables for Supersonic Flow Around Right Circular Cones at Small Angle of Attack. NASA SP-3007, National Aeronautics and Space Administration, Washington, 1964.

5. Stone, A. H. — On the Supersonic Flow Past a Slightly Yawing Cone. Part II. Journal of Mathematics and Physics, Vol. 30, No. 4, Jan. 1952, pp. 200-213.

6. Kopal, Z. — Tables of Supersonic Flow Around Cones of Large Yaw. Massachusetts Institute of Technology, Dept. of Electrical Engineering, Tech. Report No. 5, Cambridge, Mass., 1949.

7. Ferri, A. — Supersonic Flow Around Circular Cones at Angles of Attack. NACA TN 2236, National Aeronautics and Space Administration, Washington, Nov. 1950.

8. Melnik, R. E. — A Conical Thin-Shock-Layer Theory Uniformly Valid in the Entropy Layer. U.S. Air Force Flight Dynamics Lab., Report No. FDL-TDR-64-82, 1965.

9. Melnik, R. E. — Vortical Singularities in Conical Flow. AIAA Journal, Vol. 5, No. 4, 1967, pp. 631-637.

10. Stocker, P. M. Mauger, F. E. — Supersonic Flow Past Cones of General Cross Section. Journal of Fluid Mechanics, Vol. 13, Pt. 3, 1962, pp. 383-399.

11. Babenko, K. I. et al. — Three Dimensional Flow of Ideal Gas Past Smooth Bodies. NASA TT F-380, National Aeronautics and Space Administration, April 1966.

12. Gonidou, R. — Écoulements Supersoniques Autour de Cônes en Incidence. ONERA, La Recherche Aerospatiale, No. 120, Sept.-Oct., 1967, pp. 11-19.

13. Moretti, G. — Inviscid Flow Field Past a Pointed Cone at An Angle of Attack. Part I — Analysis. General Applied Science Lab., Inc., Westbury, New York, Tech. Report No. 577, Dec. 1965.

14. Hamming, R. W. Stable Predictor-Corrector Methods for Ordinary Differential Equations. Assoc. of Computing Mach. Journal, Vol. 6, No. 1, 1959, p. 37.

15. Rainbird, W. J. Turbulent Boundary Layer Growth and Separation on a Yawed 12½° Cone at Mach Numbers 1.8 and 4.25. AIAA Paper No. 68-98, American Institute of Aeronautics and Astronautics, Jan. 1968.

16. Rainbird, W. J. The External Flow Field About Yawed Circular Cones. AGARD Conference Proceedings No. 30. IN Hypersonic Boundary Layers and Flow Fields, May, 1968.

17. Rainbird, W. J. Errors in Measurement of Mean Static Pressure of a Moving Fluid due to Pressure Holes. National Research Council of Canada, DME/NAE Quarterly Bulletin No. 1967(3).

18. Martellucci, A. An Extension of the Linearised Characteristics Method for Calculating the Supersonic Flow Around Elliptic Cones. Journal of the Aerospace Sciences, Vol. 27, No. 9, Sept. 1960, p. 667.

19. Zakkay, V.
Visich, M. Jr. Experimental Pressure Distributions on Conical Elliptical Bodies at M_∞ = 3.09 and 6.0. Polytechnic Institute of Brooklyn, PIBAL Report No. 467, March 1959.

20. Modern Computing Methods. National Physical Laboratory Notes on Applied Science No. 16 HMSO London, 1961, p. 87.

21. Powell, M. J. D. A Method for Minimising a Sum of Squares of Non-Linear Functions without Calculating Derivatives. Computer Journal, Vol. 7, No. 4, Jan. 1965, pp. 303-307.

22. Babenko, K. I. Investigation of a Three-Dimensional Gas Flow Around Conic Bodies. IN International Congress of Applied Mechanics, 11th, Munich, Germany, 1964. Berlin, Springer-Verlag, 1966, pp. 749-755.

23. Lance, G. N. Numerical Methods for High Speed Computers. Iliffe, London, 1960, p. 134.

24. Jones, D. J. Use of the Computer Programme to Determine the Flow Field for Conical Flow Situations. National Research Council of Canada, NAE LTR-HA-1 (to be published).

TABLE 1

$\bar{p}$ NEAR TO THE SURFACE FOR THE CIRCULAR CONE

$M_\infty = 1.797$, $\theta_c = 12.5°$, $\alpha = 7.5°$

ξ \ ϕ	0	22.5	45	67.5	90	112.5	135	157.5	180
0.1	0.8473	0.8322	0.7919	0.7382	0.6857	0.6463	0.6230	0.6124	0.6096
0.05	0.8522	0.8361	0.7930	0.7359	0.6809	0.6412	0.6197	0.6116	0.6099
0.025	0.8537	0.8370	0.7924	0.7333	0.6769	0.6371	0.6169	0.6107	0.6099
0.0125	0.8541	0.8371	0.7916	0.7315	0.6743	0.6346	0.6152	0.6101	0.6099
0.00625	0.8542	0.8370	0.7911	0.7304	0.6729	0.6331	0.6142	0.6098	0.6099
0.003125	0.8543	0.8369	0.7908	0.7299	0.6721	0.6324	0.6137	0.6096	0.6099
1.53×10^{-6}	0.8543	0.8369	0.7905	0.7293	0.6713	0.6316	0.6132	0.6095	0.6099
Value extrapolated from $\xi = 0.003125$	0.8543	0.8369	0.7905	0.7293	0.6713	0.6316	0.6132	0.6095	0.6099

TABLE 2

COMPARISONS OF SURFACE PRESSURE AND SHOCK SHAPE BETWEEN PRESENT THEORY AND THE THEORY OF BABENKO ET AL. (REF. 11)

$M_\infty = 5$, $\theta_c = 10$, $\alpha = 7.5$

ϕ	0	22.5	45	67.5	90	112.5	135	157.5	180
$\bar{p}_J$	0.6170	0.5872	0.5081	0.4046	0.3044	0.2284	0.1894	0.1822	0.1833
$\bar{p}_B$	0.6172	0.5874	0.5082	0.4047	0.3045	0.2284	0.1895	0.1821	0.1830
F_J	0.2488	0.2507	0.2567	0.2674	0.2832	0.3041	0.3281	0.3499	0.3596
F_B	0.2489	0.2508	0.2568	0.2674	0.2831	0.3040	0.3281	0.3495	0.3652

TABLE 3

$M_\infty = 2$, $\theta_c = 10$, $\alpha = 2.5$

ϕ	0	22.5	45	67.5	90	112.5	135	157.5	180
$\bar{p}_J$	0.6569	0.6530	0.6421	0.6271	0.6115	0.5981	0.5885	0.5831	0.5814
$\bar{p}_B$	0.6565	0.6525	0.6416	0.6265	0.6109	0.5976	0.5882	0.5829	0.5812
F_J	0.5601	0.5633	0.5724	0.5867	0.6046	0.6236	0.6407	0.6527	0.6570
F_B	0.5624	0.5655	0.5746	0.5889	0.6067	0.6256	0.6426	0.6546	0.6588

Subscripts: J Values obtained by present method

B Values obtained by Babenko et al. (Ref. 11)

TABLE 4

COMPARISONS OF SURFACE PRESSURE AND SHOCK SHAPE BETWEEN PRESENT THEORY AND THE THEORY OF BABENKO ET AL. (REF. 11)

$M_\infty = 2, \theta_c = 15, \alpha = 10$

ϕ	0	22.5	45	67.5	90	112.5	135	157.5	180
$\bar{p}_J$	1.0143	0.9839	0.9018	0.7931	0.6884	0.6153	0.5833	0.5783	0.5795
$\bar{p}_B$	1.0153	0.9852	0.9039	0.7957	0.6914	0.6178	0.5852	0.5805	0.5821
F_J	0.5624	0.5691	0.5896	0.6244	0.6737	0.7351	0.8010	0.8550	0.8764
F_B	0.5636	0.5703	0.5909	0.6259	0.6755	0.7369	0.8037	0.8574	0.8795

TABLE 5

$M_\infty = 5, \theta_c = 15, \alpha = 10$

ϕ	0	22.5	45	67.5	90	112.5	135	157.5	180
$\bar{p}_J$	1.0698	1.0141	0.8667	0.6750	0.4897	0.3469	0.2624	0.2333	0.2303
$\bar{p}_B$	1.0700	1.0144	0.8668	0.6748	0.4897	0.3467	0.2623	0.2334	0.2296
F_J	0.3459	0.3476	0.3530	0.3623	0.3763	0.3942	0.4142	0.4298	0.4366
F_B	0.3460	0.3477	0.3530	0.3624	0.3763	0.3943	0.4140	0.4302	0.4363

Subscripts: J Values obtained by present method

B Values obtained by Babenko et al. (Ref. 11)

TABLE 6

COMPARISONS OF SURFACE PRESSURE AND SHOCK SHAPE BETWEEN PRESENT THEORY AND THE THEORY OF BABENKO ET AL. (REF. 11)

$M_\infty = 7, \theta_c = 15, \alpha = 10$

ϕ	0	22.5	45	67.5	90	112.5	135	157.5	180
$\bar{p}_J$	1.0795	1.0178	0.8542	0.6435	0.4426	0.2901	0.1972	0.1615	0.1562
$\bar{p}_B$	1.0798	1.0179	0.8544	0.6433	0.4426	0.2899	0.1974	0.1615	0.1560
F_J	0.3260	0.3271	0.3304	0.3363	0.3450	0.3561	0.3681	0.3755	0.3772
F_B	0.3261	0.3272	0.3305	0.3363	0.3449	0.3561	0.3679	0.3753	0.3776

Subscripts: J Values obtained by present method

B Values obtained by Babenko et al. (Ref. 11)

TABLE 7

COMPARISONS OF SURFACE VALUES AND SHOCK SHAPE BETWEEN PRESENT THEORY AND THE THEORY OF BABENKO ET AL. (REF. 11)

$M_\infty = 5$, $\theta_c = 25$, $\alpha = 20$

ϕ	0	22.5	45	67.5	90	112.5	135	157.5	180
$\bar{u}_J$	1.3028	1.3167	1.3571	1.4205	1.5026	1.5956	1.6906	1.7741	1.8123
$\bar{u}_B$	1.3026	1.3165	1.3572	1.4217	1.5048	1.5989	1.6936	1.7711	1.8129
$\bar{v}_J$	0.6075	0.6140	0.6328	0.6624	0.7007	0.7440	0.7883	0.8273	0.8451
$\bar{v}_B$	0.6074	0.6139	0.6329	0.6630	0.7017	0.7456	0.7897	0.8259	0.8454
$\bar{w}_J$	0	0.1785	0.3464	0.4862	0.5890	0.6358	0.6205	0.4319	0
$\bar{w}_B$	0	0.1792	0.3446	0.4832	0.5818	0.6285	0.6075	0.4463	0
$\bar{p}_J$	2.6838	2.5058	2.0418	1.4619	0.9277	0.5447	0.3172	0.2426	0.2522
$\bar{p}_B$	2.6842	2.5062	2.0423	1.4596	0.9282	0.5434	0.3182	0.2436	0.2508
$\bar{\rho}_J$	4.7758	4.5474	3.9284	3.0946	2.2362	1.5288	1.0391	0.8580	0.8819
$\bar{\rho}_B$	4.7759	4.5475	3.9289	3.0909	2.2368	1.5260	1.0411	0.8603	0.8785
F_J	0.5919	0.5943	0.6029	0.6168	0.6395	0.6657	0.6960	0.7075	0.6920
F_B	0.5920	0.5947	0.6028	0.6173	0.6388	0.6665	0.6949	0.7068	0.6917

Subscripts: J Values obtained by present method

B Values obtained by Babenko et al. (Ref. 11)

TABLE 8

COMPARISONS OF SURFACE VALUES AND SHOCK SHAPE BETWEEN PRESENT THEORY AND THE THEORY OF BABENKO ET AL. (REF. 11)

$M_\infty = 7, \theta_c = 10, \alpha = 5$

ϕ	0	22.5	45	67.5	90	112.5	135	157.5	180
$\bar{u}_J$	2.1933	2.1952	2.2009	2.2099	2.2212	2.2336	2.2451	2.2535	2.2565
$\bar{u}_B$	2.1932	2.1952	2.2009	2.2099	2.2213	2.2338	2.2453	2.2536	2.2565
$\bar{v}_J$	0.3867	0.3871	0.3881	0.3897	0.3917	0.3938	0.3959	0.3974	0.3979
$\bar{v}_B$	0.3867	0.3871	0.3881	0.3897	0.3917	0.3939	0.3959	0.3974	0.3979
$\bar{w}_J$	0	0.0579	0.1107	0.1535	0.1801	0.1838	0.1546	0.0885	0
$\bar{w}_B$	0	0.0578	0 1104	0.1526	0.1786	0.1801	0.1504	0.0861	0
$\bar{p}_J$	0.4646	0.4457	0.3952	0.3273	0.2594	0.2042	0.1688	0.1522	0.1479
$\bar{p}_B$	0.4647	0.4459	0.3952	0.3274	0.2594	0.2043	0.1689	0.1522	0.1479
$\bar{\rho}_J$	3.1270	3.0359	2.7857	2.4352	2.0622	1.7386	1.5174	1.4094	1.3808
$\bar{\rho}_B$	3.1275	3.0364	2.7858	2.4354	2.0620	1.7386	1.5179	1.4090	1.3804
F_J	0.2284	0.2293	0.2322	0.2371	0.2440	0.2526	0.2615	0.2687	0.2715
F_B	0.2285	0.2294	0.2323	0.2372	0.2440	0.2525	0.2614	0.2691	0.2719

Subscripts: J Values obtained by present method

B Values obtained by Babenko et al. (Ref. 11)

TABLE 9

COMPARISONS OF SURFACE VALUES AND SHOCK SHAPE BETWEEN PRESENT THEORY AND THE THEORY OF BABENKO ET AL. (REF. 11)

$M_\infty = 5, \theta_c = 10, \alpha = 5$

ϕ	0	22.5	45	67.5	90	112.5	135	157.5	180
$\bar{u}_J$	2.0911	2.0934	2.1001	2.1106	2.1238	2.1381	2.1512	2.1604	2.1637
$\bar{u}_B$	2.0911	2.0934	2.1001	2.1107	2.1239	2.1382	2.1513	2.1604	2.1637
$\bar{v}_J$	0.3687	0.3691	0.3703	0.3722	0.3745	0.3770	0.3793	0.3809	0.3815
v_B	0.3687	0.3691	0.3703	0.3722	0.3745	0.3770	0.3793	0.3809	0.3815
$\bar{w}_J$	0	0.0681	0.1301	0.1798	0.2095	0.2102	0.1723	0.0963	0
$\bar{w}_B$	0	0.0678	0.1295	0.1788	0.2084	0.2090	0.1719	0.0971	0
$\bar{p}_J$	0.5053	0.4882	0.4421	0.3797	0.3169	0.2665	0.2353	0.2215	0.2181
$\bar{p}_B$	0.5055	0.4884	0.4422	0.3798	0.3169	0.2665	0.2352	0.2214	0.2180
$\bar{\rho}_J$	2.3721	2.3144	2.1559	1.9342	1.6998	1.5020	1.3742	1.3162	1.3018
$\bar{\rho}_B$	2.3726	2.3149	2.1562	1.9344	1.6997	1.5017	1.3735	1.3154	1.3009
F_J	0.2557	0.2573	0.2620	0.2699	0.2810	0.2946	0.3088	0.3206	0.3253
F_B	0.2558	0.2573	0.2620	0.2699	0.2810	0.2945	0.3090	0.3206	0.3252

Subscripts: J Values obtained by present method

B Values obtained by Babenko et al. (Ref. 11)

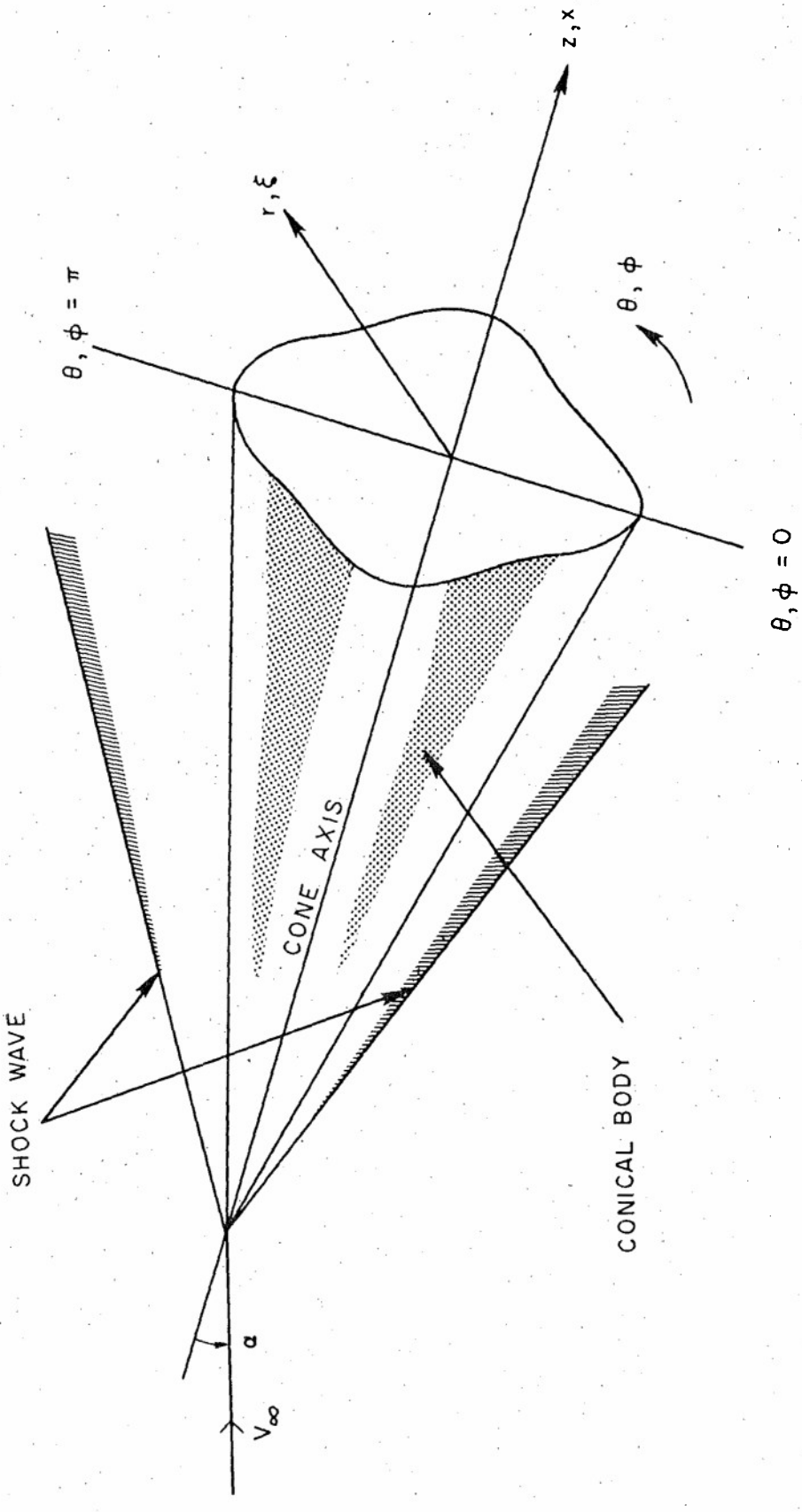

FIG. 1: CO-ORDINATE SYSTEMS

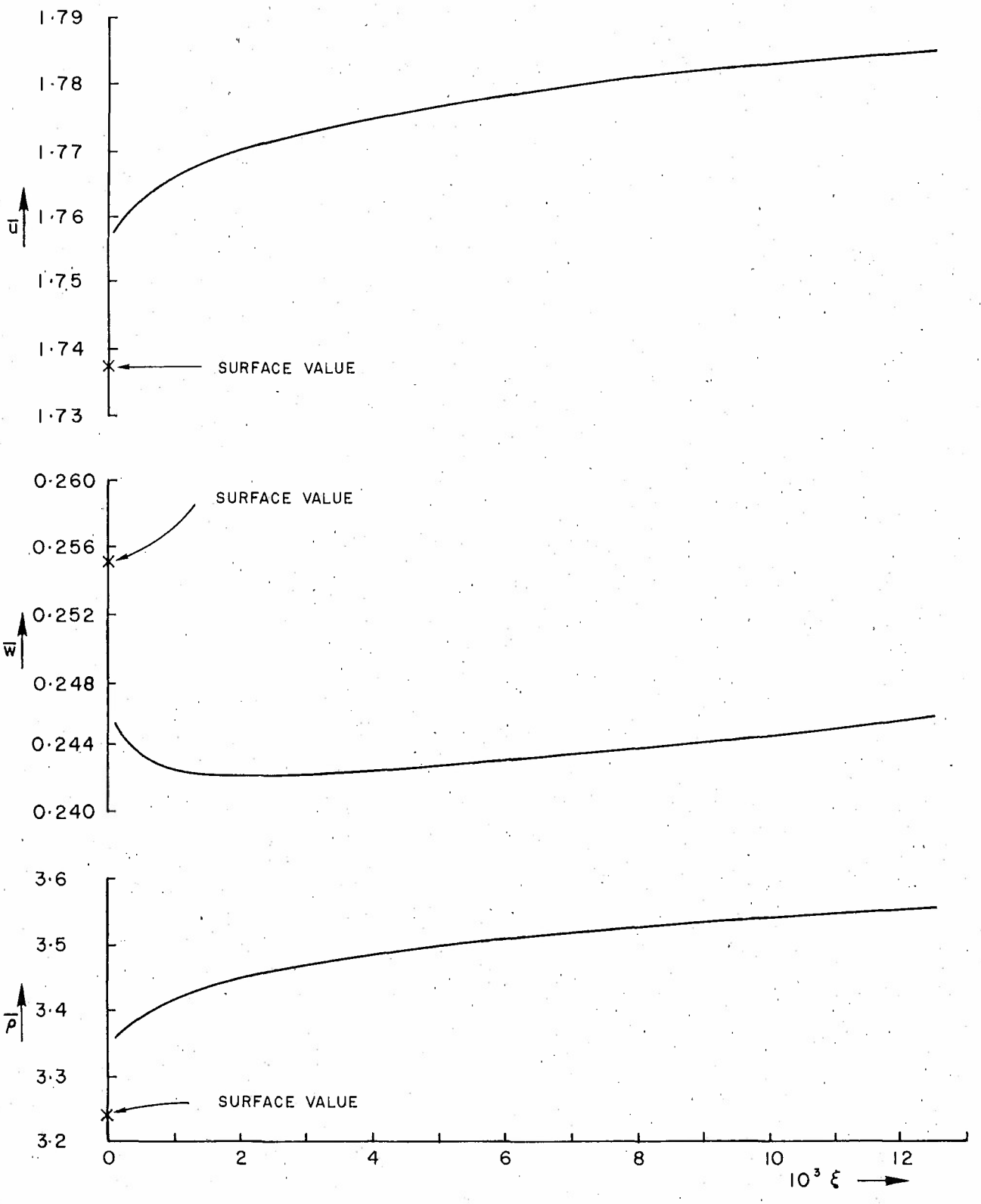

FIG. 2 : CIRCULAR CONE
PLOTS OF $\bar{u}$, $\bar{w}$ AND $\bar{\rho}$ NEAR TO THE SURFACE AT $\phi = 90°$

$M_\infty = 7$, $\theta_c = 25$, $\alpha = 10°$

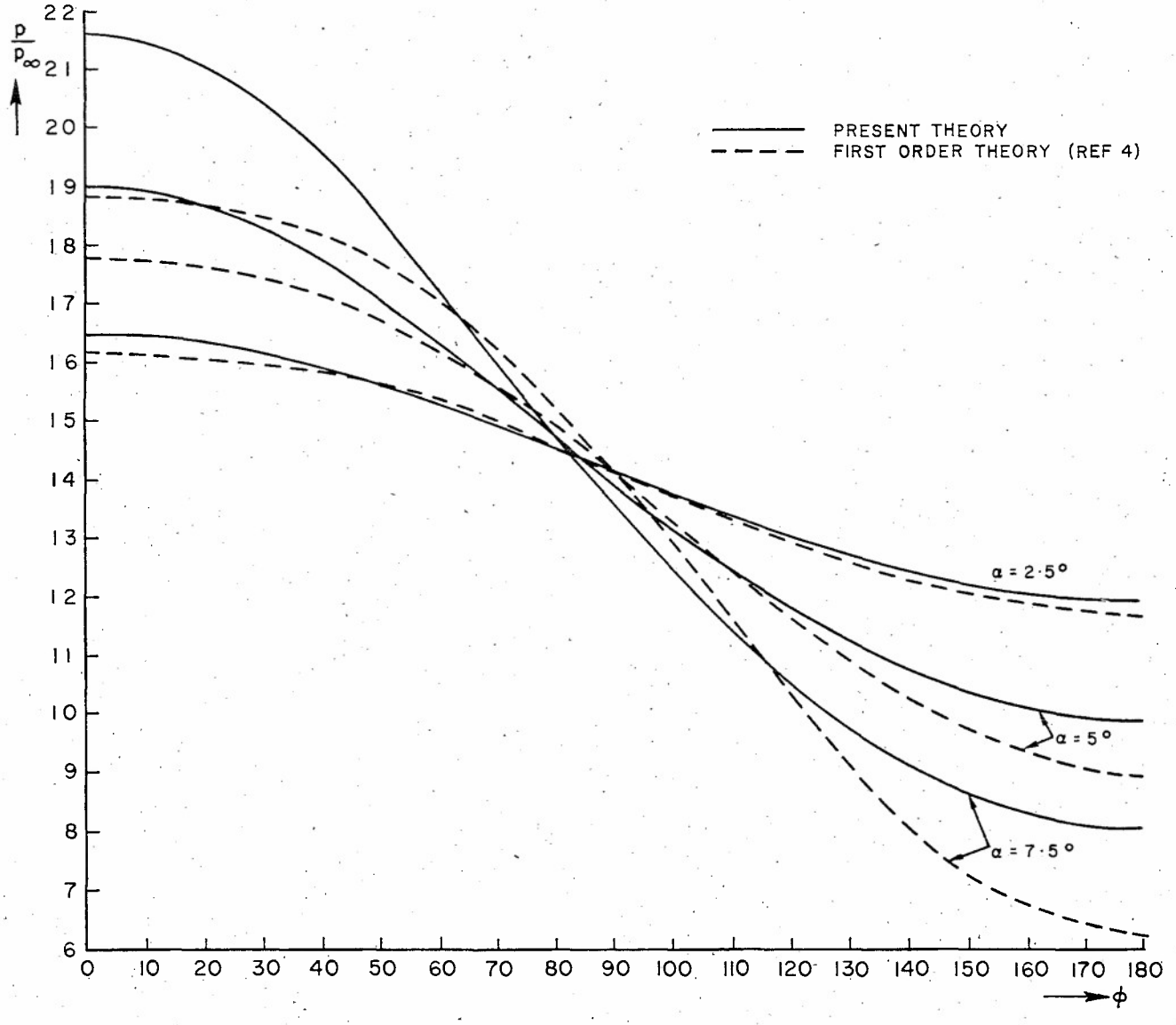

FIG. 3: CIRCULAR CONE
PLOTS OF FIRST ORDER AND PRESENT SURFACE PRESSURE RESULTS

$M_\infty = 7 \quad \theta_c = 25°$

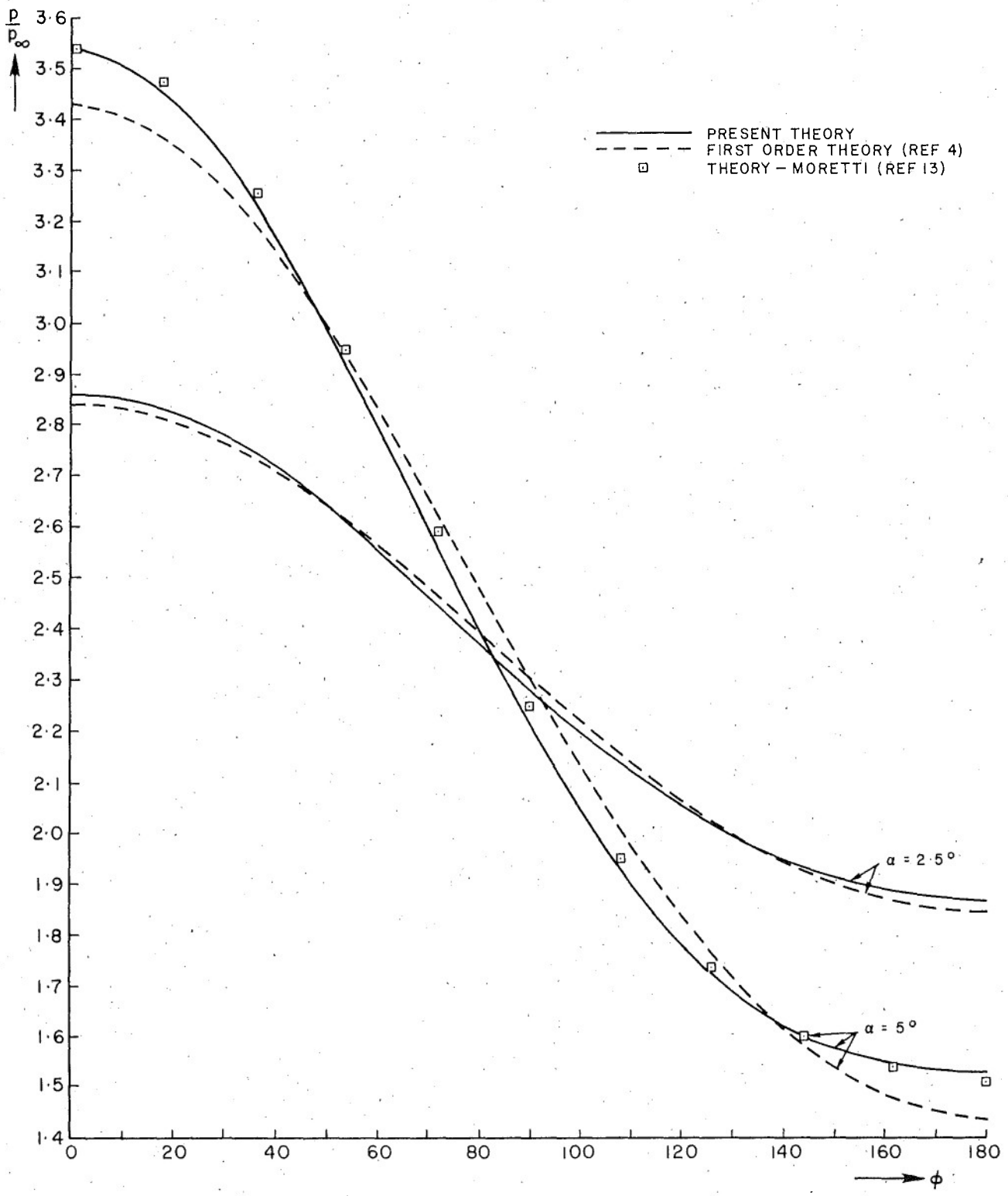

FIG. 4: CIRCULAR CONE
PLOTS OF FIRST ORDER, MORETTI'S, AND PRESENT SURFACE PRESSURE RESULTS.

$M_\infty = 5$ $\theta_c = 10°$

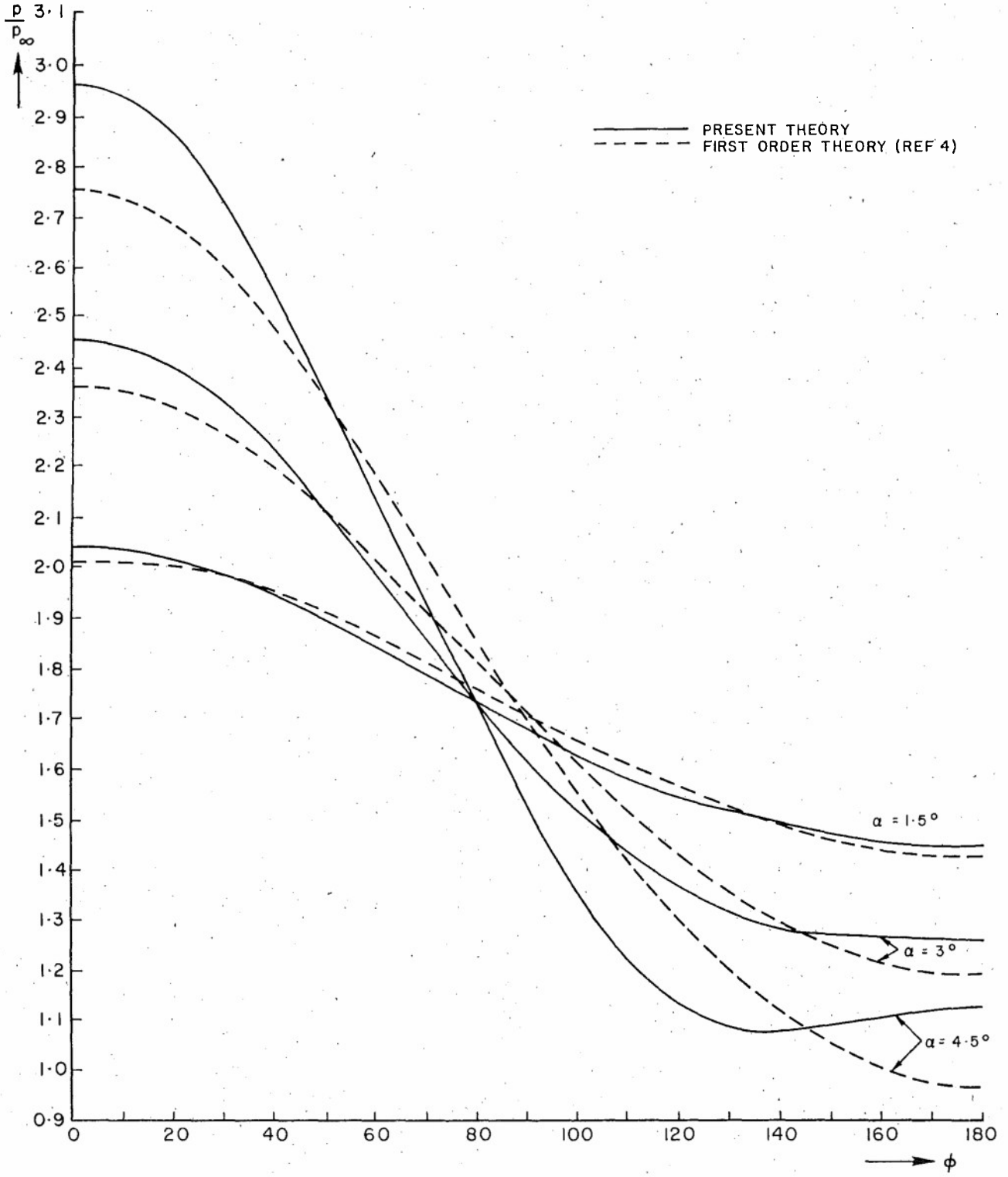

FIG. 5 : CIRCULAR CONE
PLOTS OF FIRST ORDER AND PRESENT SURFACE PRESSURE RESULTS

$M_\infty = 7$ $\theta_c = 5°$

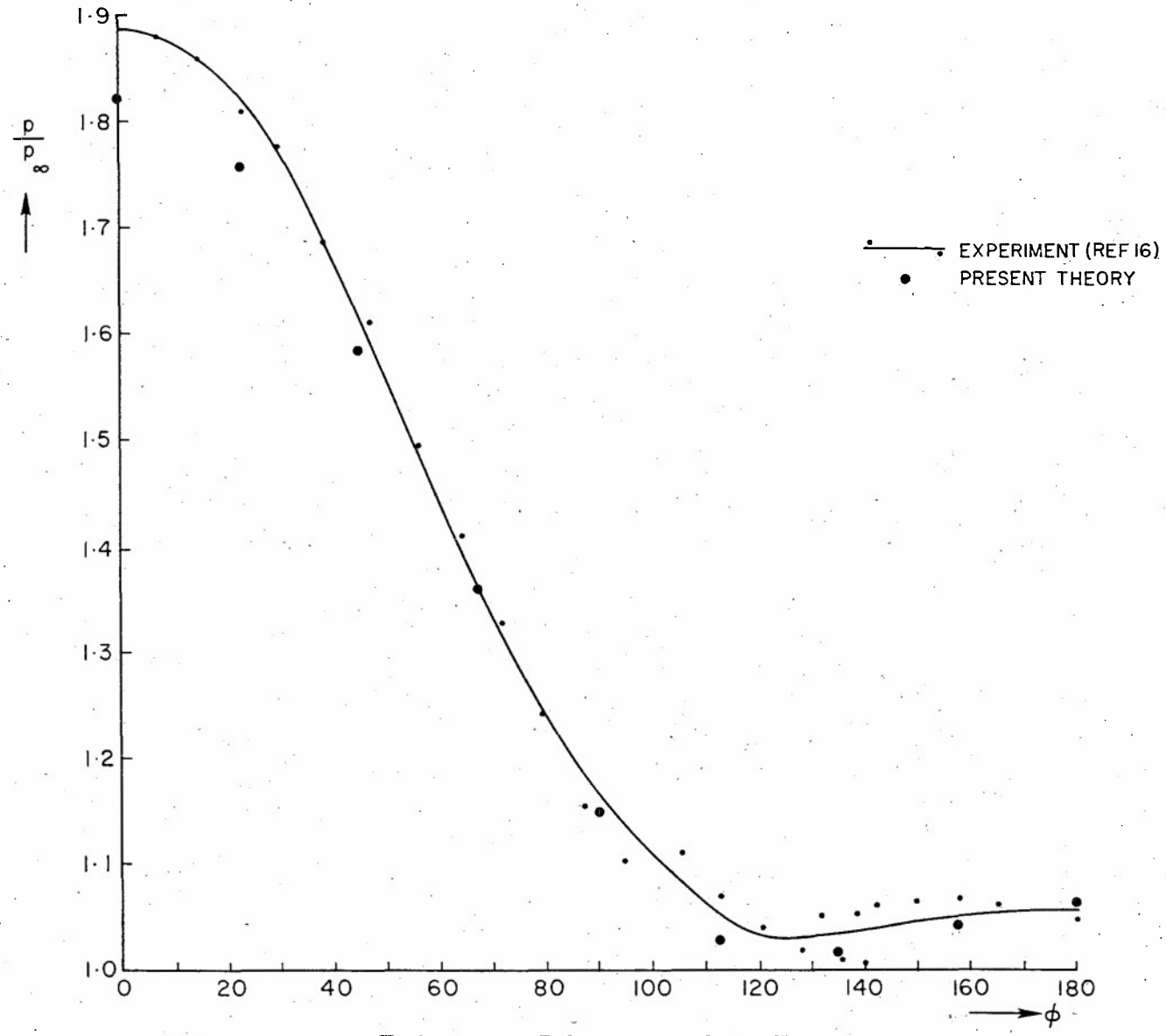

FIG. 6: CIRCULAR CONE
COMPARISON OF SURFACE PRESSURE BETWEEN PRESENT THEORY AND EXPERIMENT
$M_\infty = 4{\cdot}25$, $\theta_c = 5°$, $\alpha = 5°$

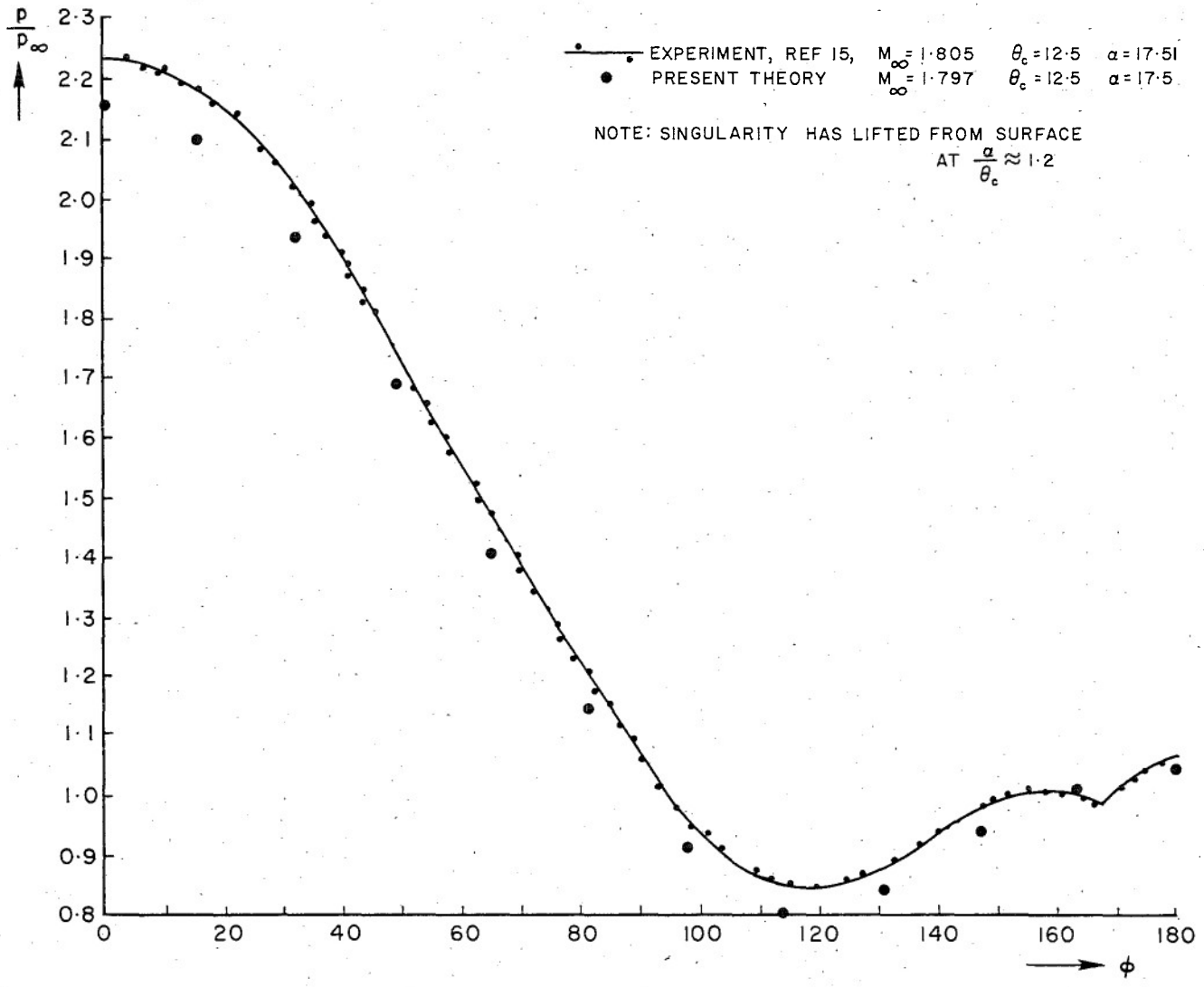

FIG. 7: CIRCULAR CONE
COMPARISON OF SURFACE PRESSURE BETWEEN PRESENT THEORY AND EXPERIMENT

$M_\infty = 1{\cdot}8 \quad \theta_c = 12{\cdot}5° \quad \alpha = 17{\cdot}5°$

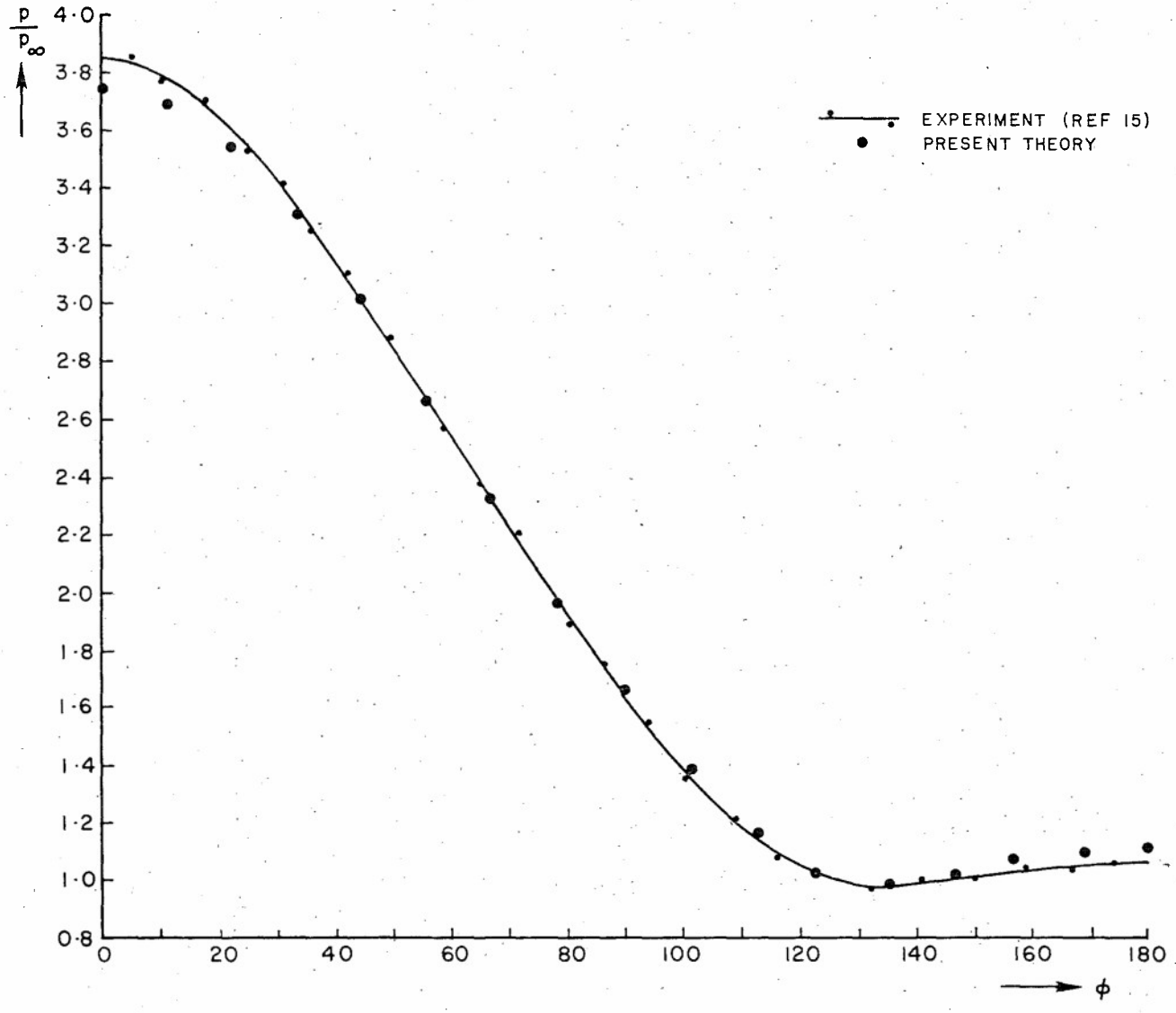

FIG. 8 : CIRCULAR CONE
COMPARISON OF SURFACE PRESSURE BETWEEN PRESENT THEORY AND EXPERIMENT

$M_\infty = 3{\cdot}26 \quad \theta_c = 12{\cdot}5° \quad \alpha = 12{\cdot}5°$

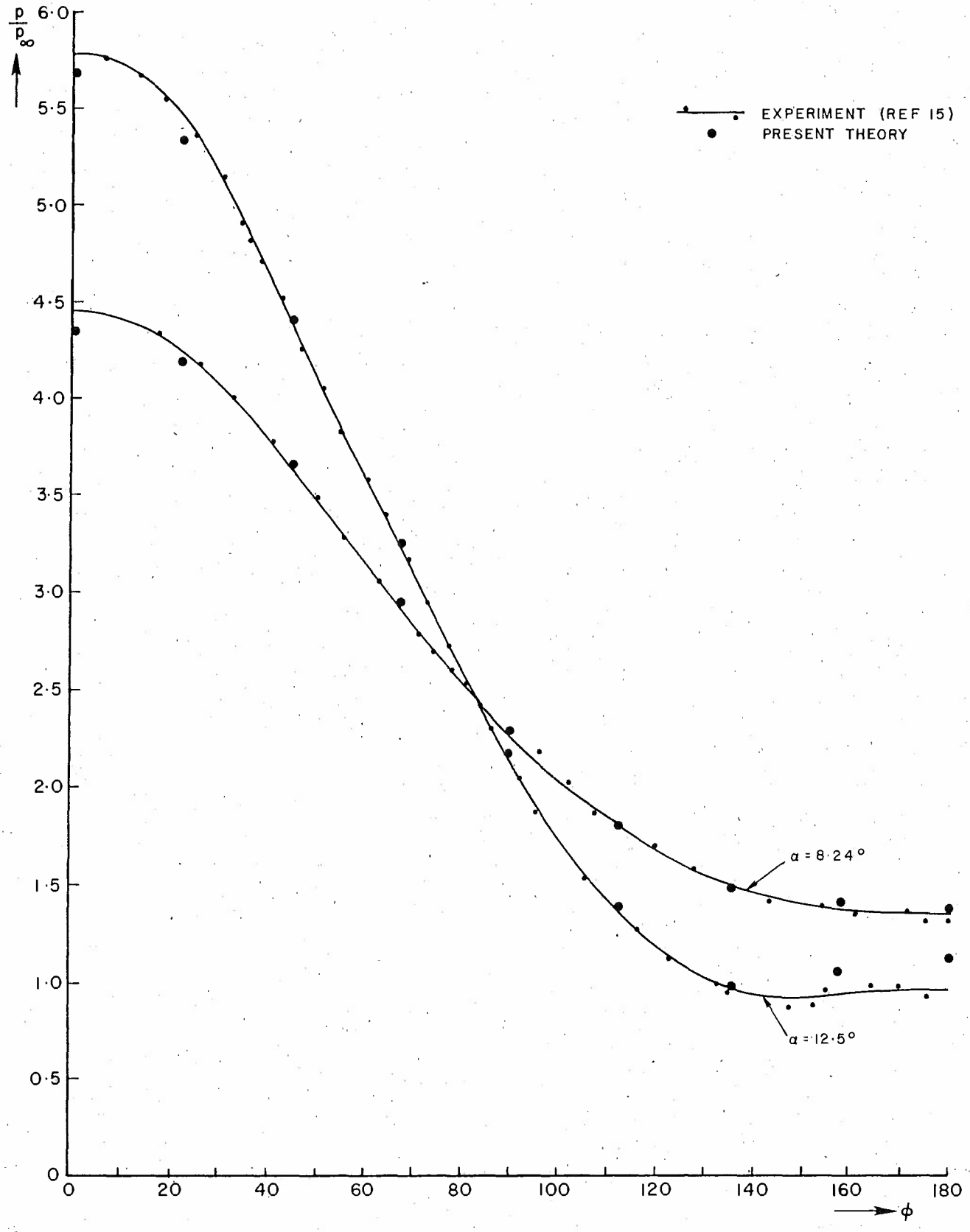

FIG. 9: CIRCULAR CONE
COMPARISON OF SURFACE PRESSURE BETWEEN PRESENT THEORY AND EXPERIMENT

$M_\infty = 4{\cdot}25$, $\theta_c = 12{\cdot}5°$, $\alpha = 8{\cdot}24°$ AND $12{\cdot}5°$

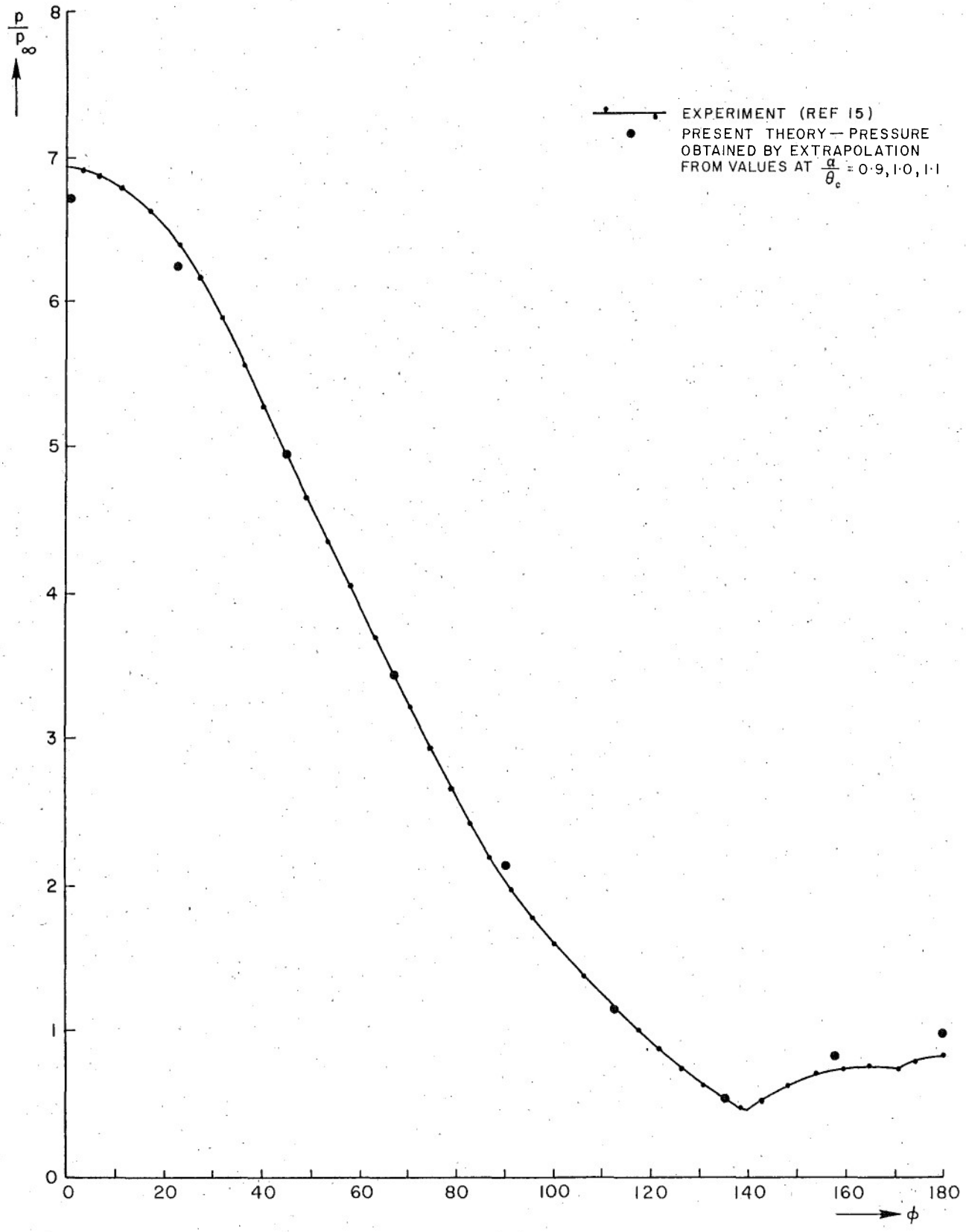

FIG. 10: CIRCULAR CONE
COMPARISON OF SURFACE PRESSURE BETWEEN PRESENT THEORY AND EXPERIMENT

$M_\infty = 4{\cdot}25$, $\theta_c = 12{\cdot}5°$, $\alpha = 15{\cdot}63°$

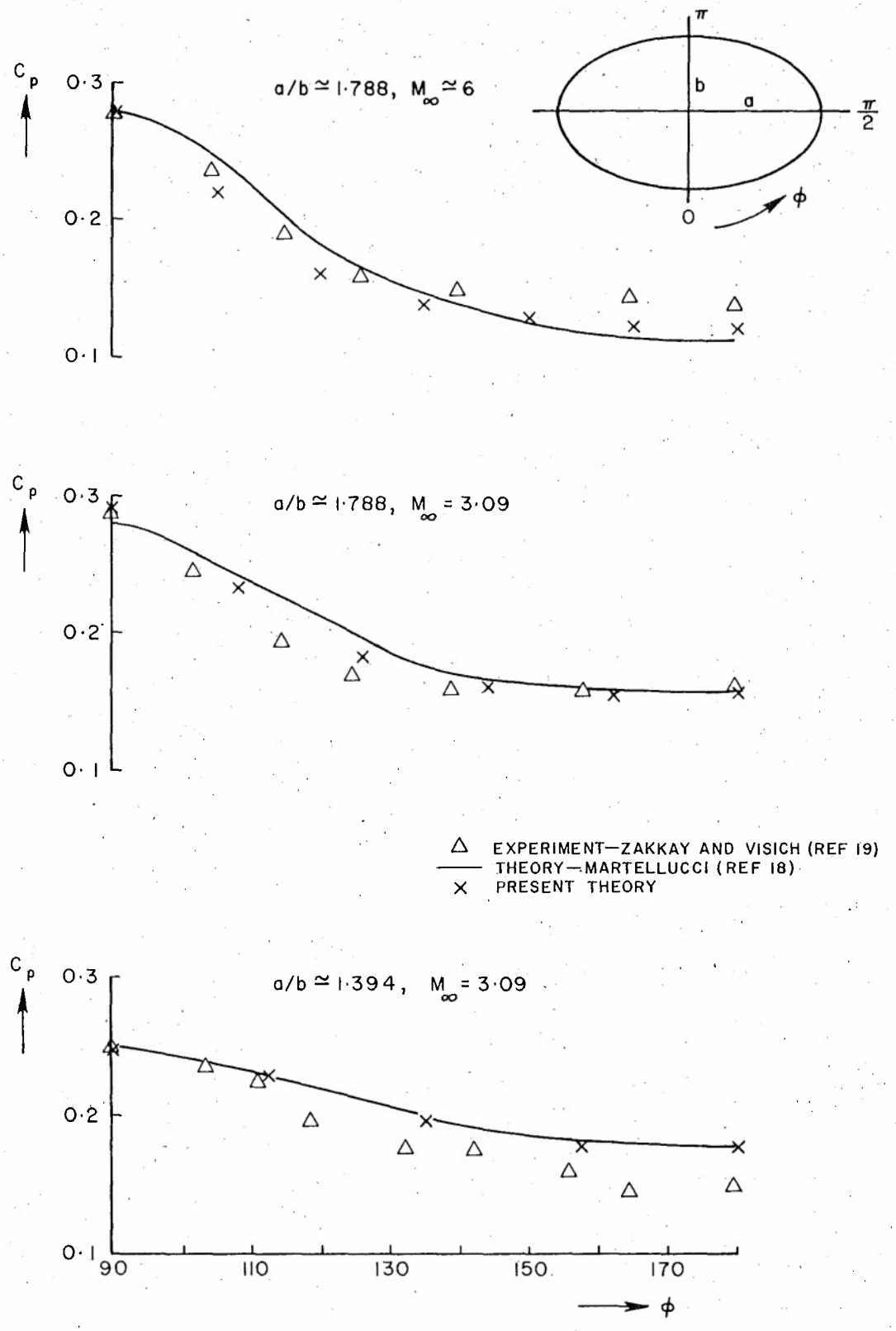

FIG. 11: ELLIPTIC CONE
COMPARISON OF SURFACE PRESSURE BETWEEN PRESENT THEORY, THEORY OF MARTELLUCCI, AND EXPERIMENT
$\sqrt{ab}$ = 0·3017, α = 0°

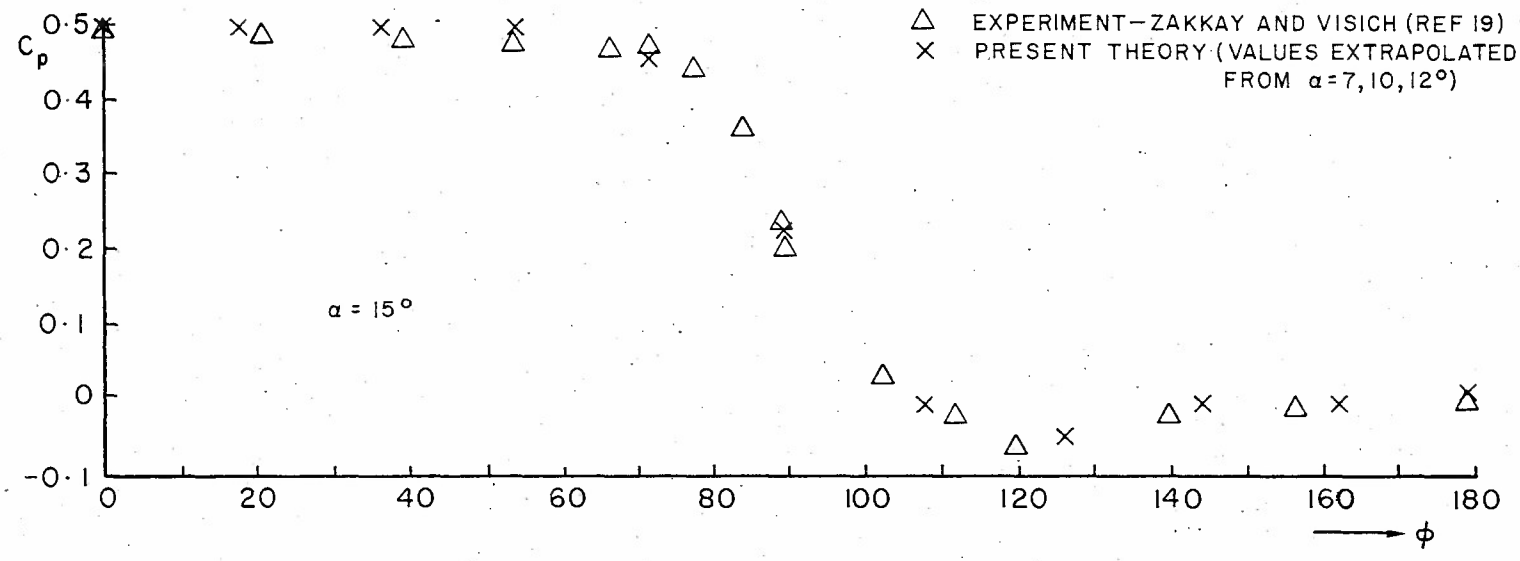

FIG.12a: ELLIPTIC CONE
COMPARISON OF SURFACE PRESSURE BETWEEN PRESENT THEORY AND EXPERIMENT

$\sqrt{ab}$ = 0·3017, M_∞ = 3·09, a/b = 1·788

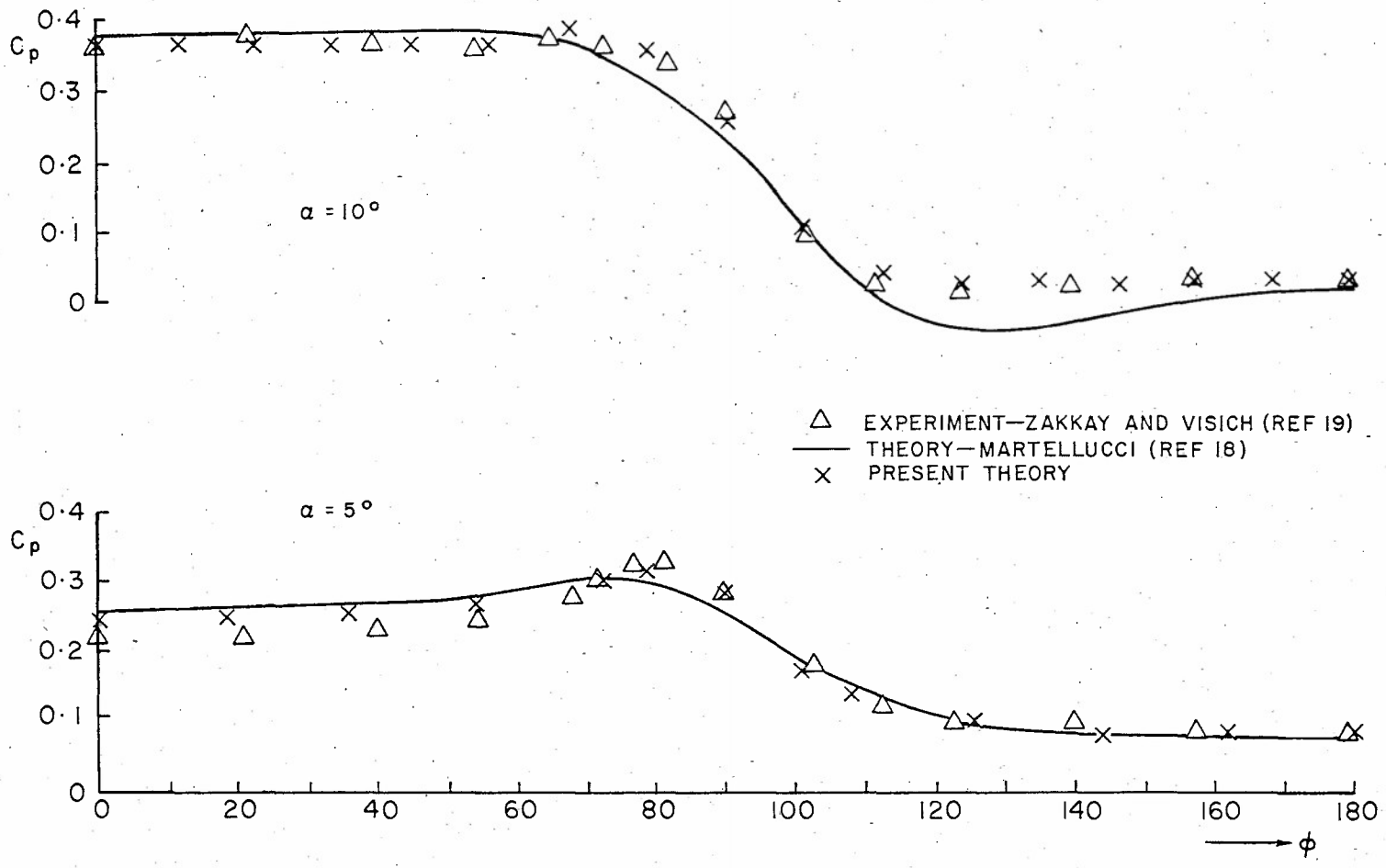

FIG. 12b: ELLIPTIC CONE
COMPARISON OF SURFACE PRESSURE BETWEEN PRESENT THEORY, THEORY OF MARTELLUCCI, AND EXPERIMENT

$\sqrt{ab}$ = 0·3017, M_∞ = 3·09, a/b = 1·788

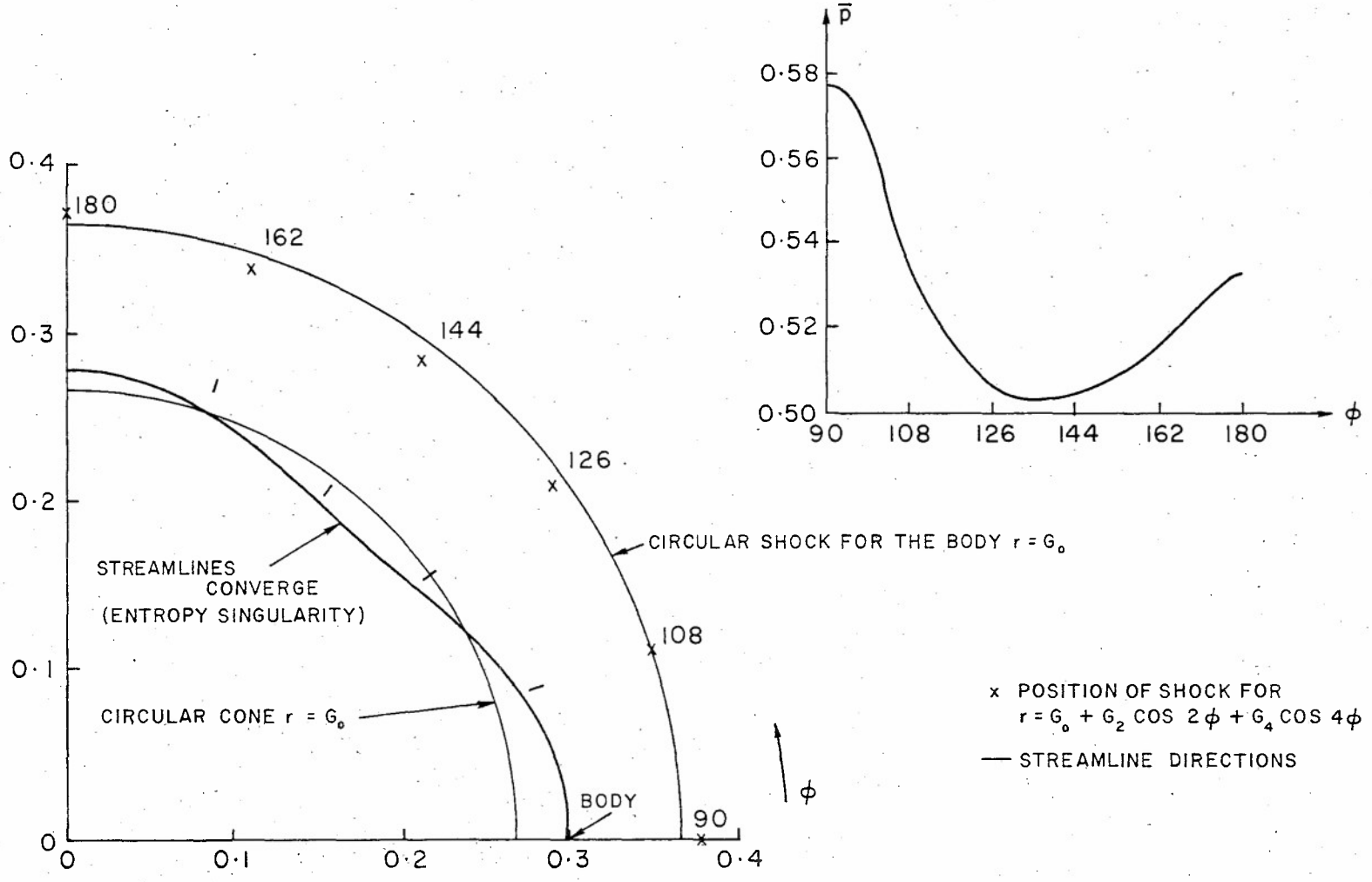

FIG. 13: BODY GIVEN BY $r = G_0 + G_2 \cos 2\phi + G_4 \cos 4\phi$ ($G_0 = 0{\cdot}2679$, $G_2 = -0{\cdot}01$, $G_4 = 0{\cdot}02$)

SHOCK SHAPE AND PRESSURE DISTRIBUTION FOR $M_\infty = 5$, $\alpha = 0°$
SOLUTION STARTED FROM CIRCULAR CONE $r = G_0$ AND BODY
ALTERED BY CHANGING G_2, G_4

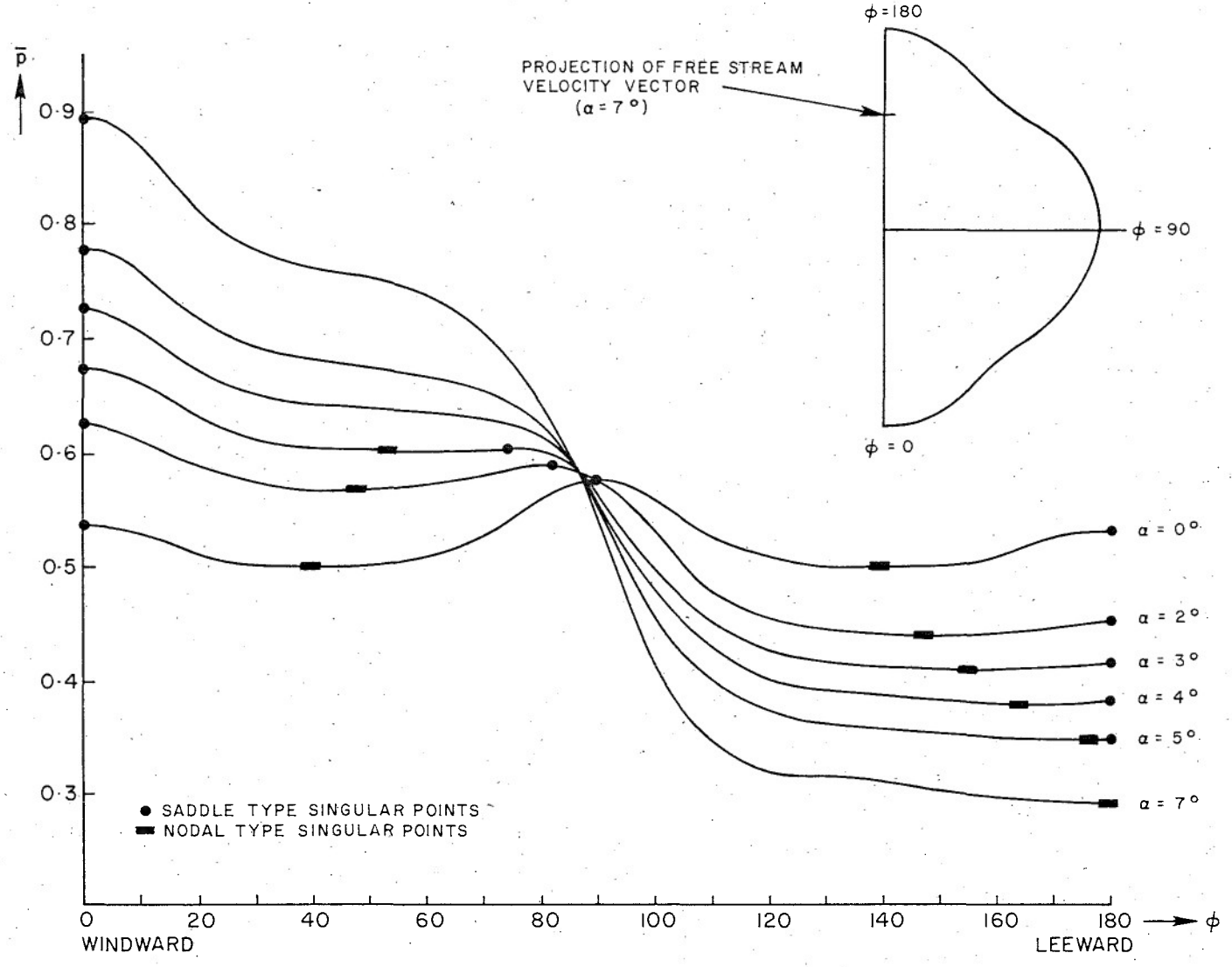

FIG. 14: BODY GIVEN BY $r = G_0 + G_2 \cos 2\phi + G_4 \cos 4\phi$ ($G_0 = 0{\cdot}2679, G_2 = -0{\cdot}01, G_4 = 0{\cdot}02$ AT UNIT DISTANCE FROM APEX)

$M_\infty = 5$, SURFACE PRESSURE DISTRIBUTIONS FOR VARIOUS INCIDENCES

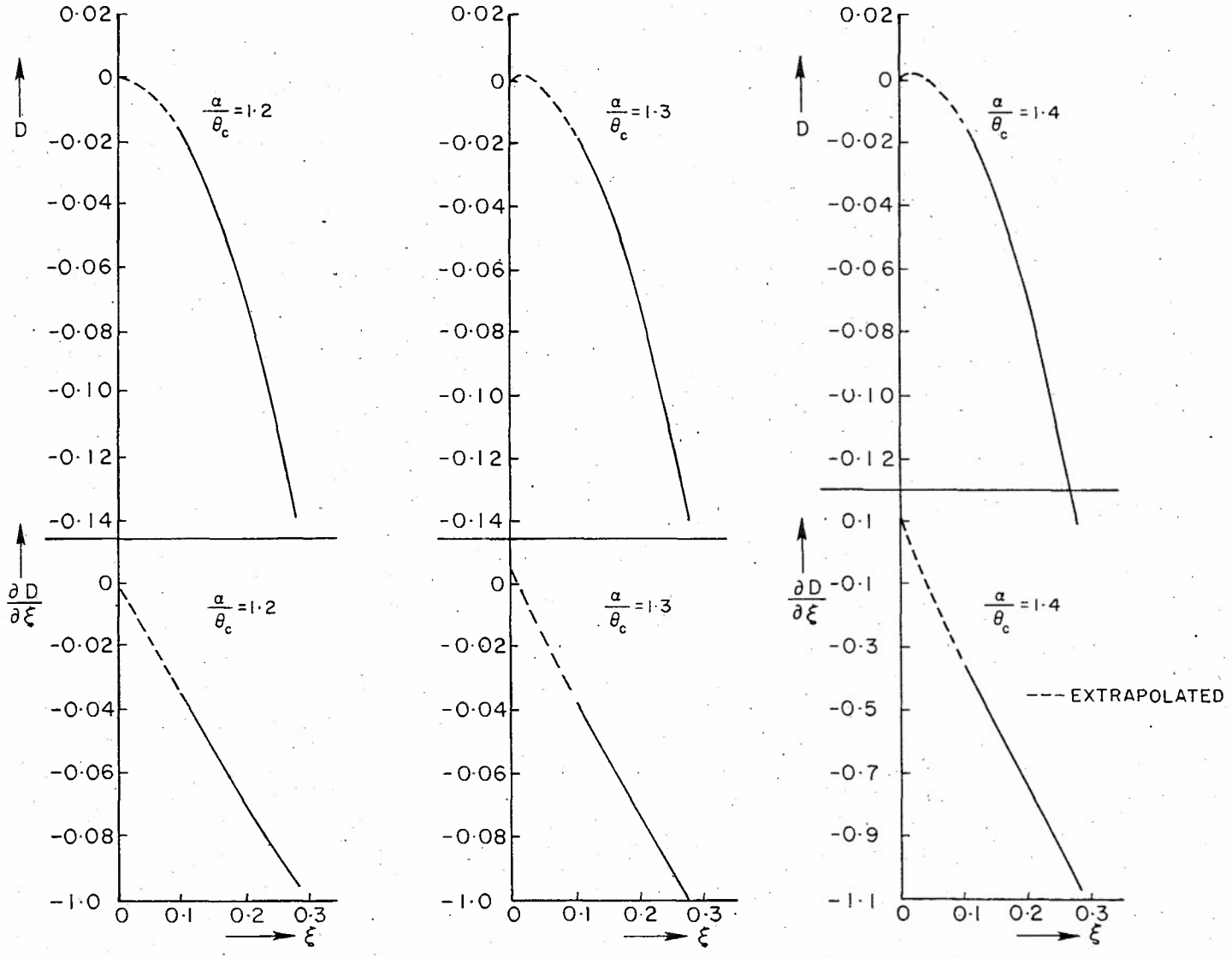

FIG. 15: CIRCULAR CONE

PLOTS OF $D = \frac{r}{\xi_r}(\xi_z u + \xi_r v)$ AND $\frac{\partial D}{\partial \xi}$ ALONG LEEWARD PLANE OF SYMMETRY ($\phi = \pi$)

ENTROPY SINGULARITY IS SITUATED WHERE $\frac{r}{\xi_r}(\xi_z u + \xi_r v) = 0$

$M_\infty = 1·797 \quad \theta_c = 12·5°$

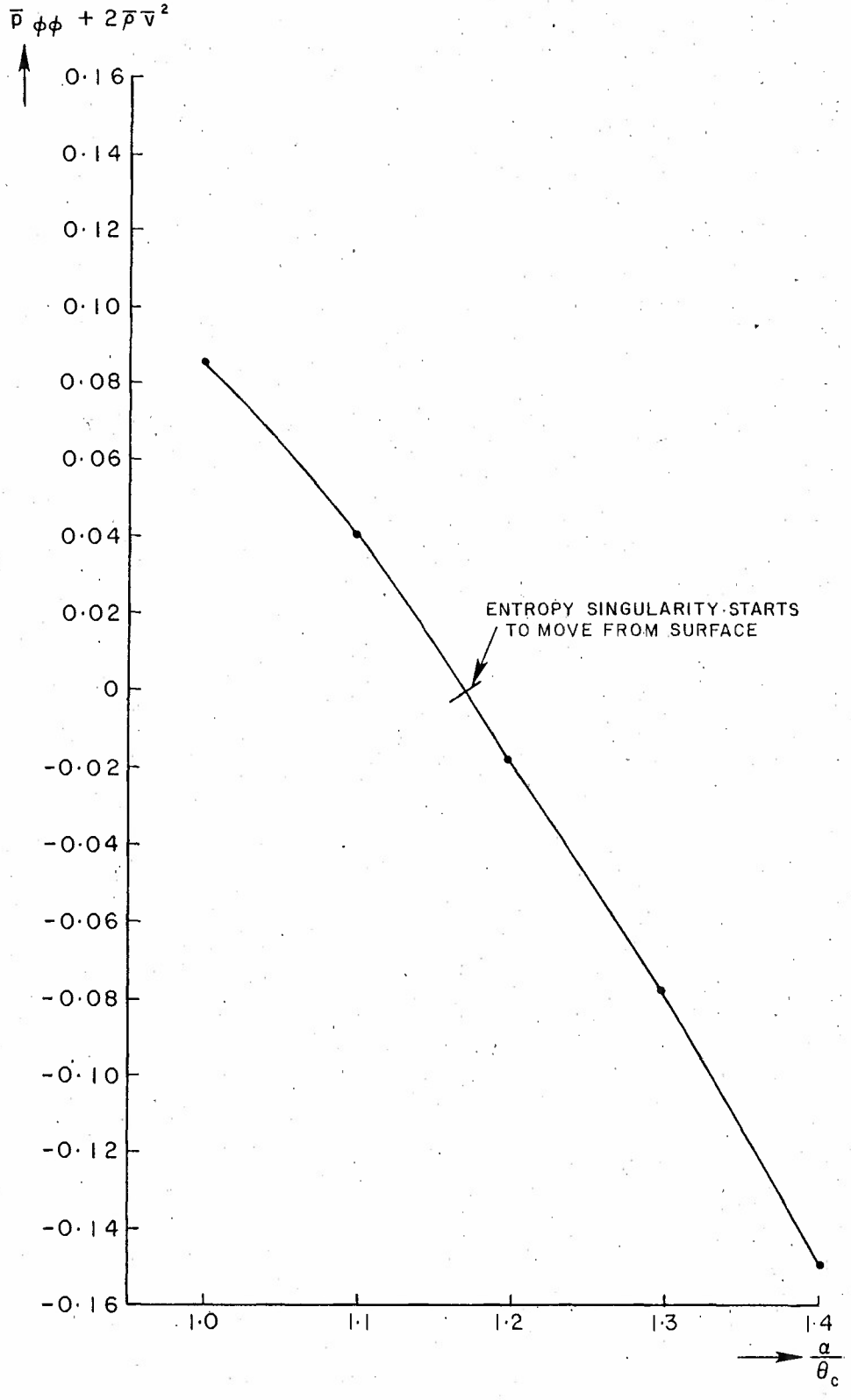

FIG. 16: CIRCULAR CONE
PLOT OF $\bar{p}_{\phi\phi}+2\bar{p}\bar{v}^2$ AT THE LEEWARD GENERATOR $\phi = \pi$ (USING ISENTROPIC SURFACE VALUES) AGAINST RELATIVE INCIDENCE $\frac{\alpha}{\theta_c}$ FOR THE CASE
$M_\infty = 1{\cdot}797 \qquad \theta_c = 12{\cdot}5°$

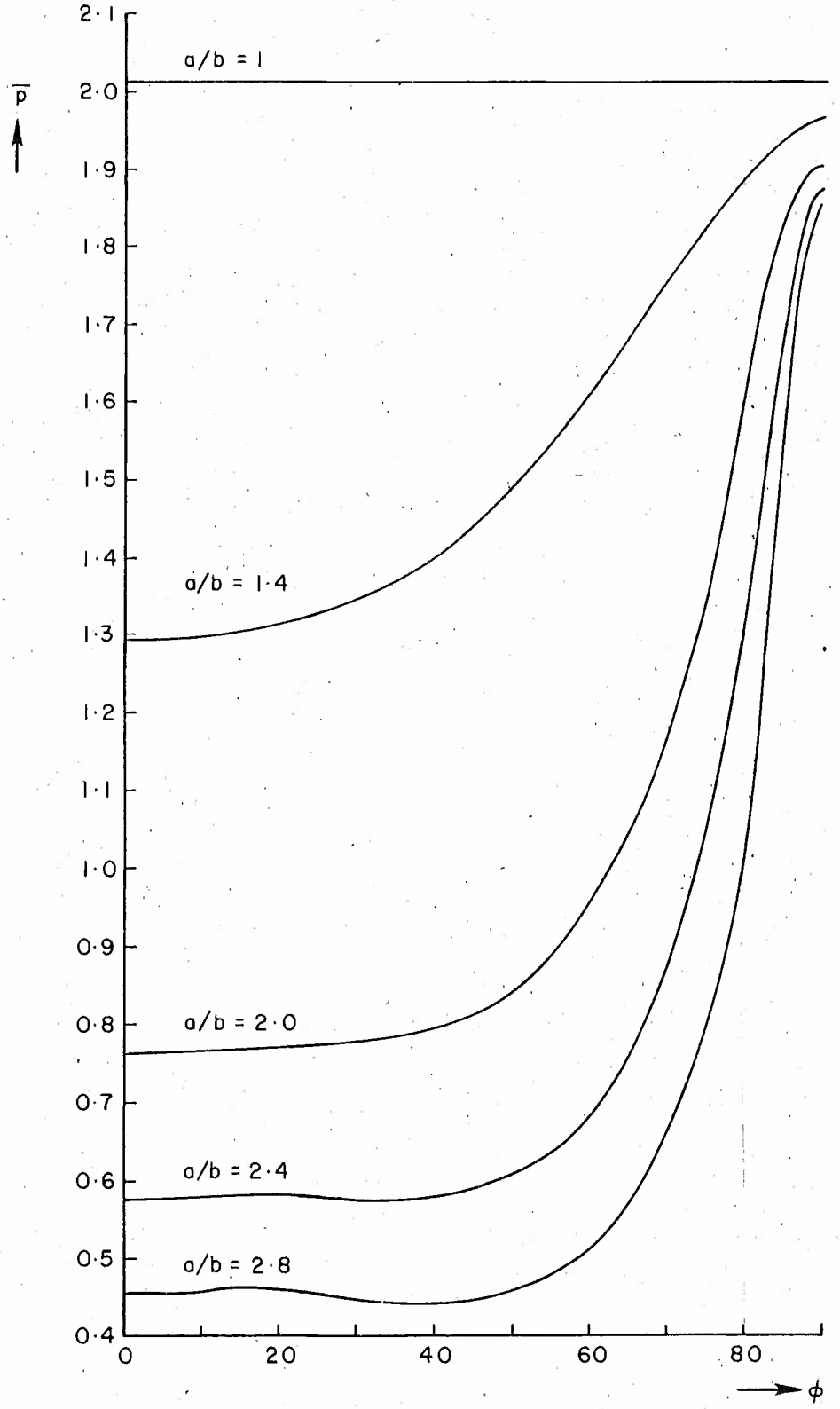

FIG. 17: ELLIPTIC CONE
PRESSURE DISTRIBUTION AROUND ELLIPTIC CONES AT ZERO INCIDENCE

$M_\infty = 10$ $\alpha = 0{\cdot}7$

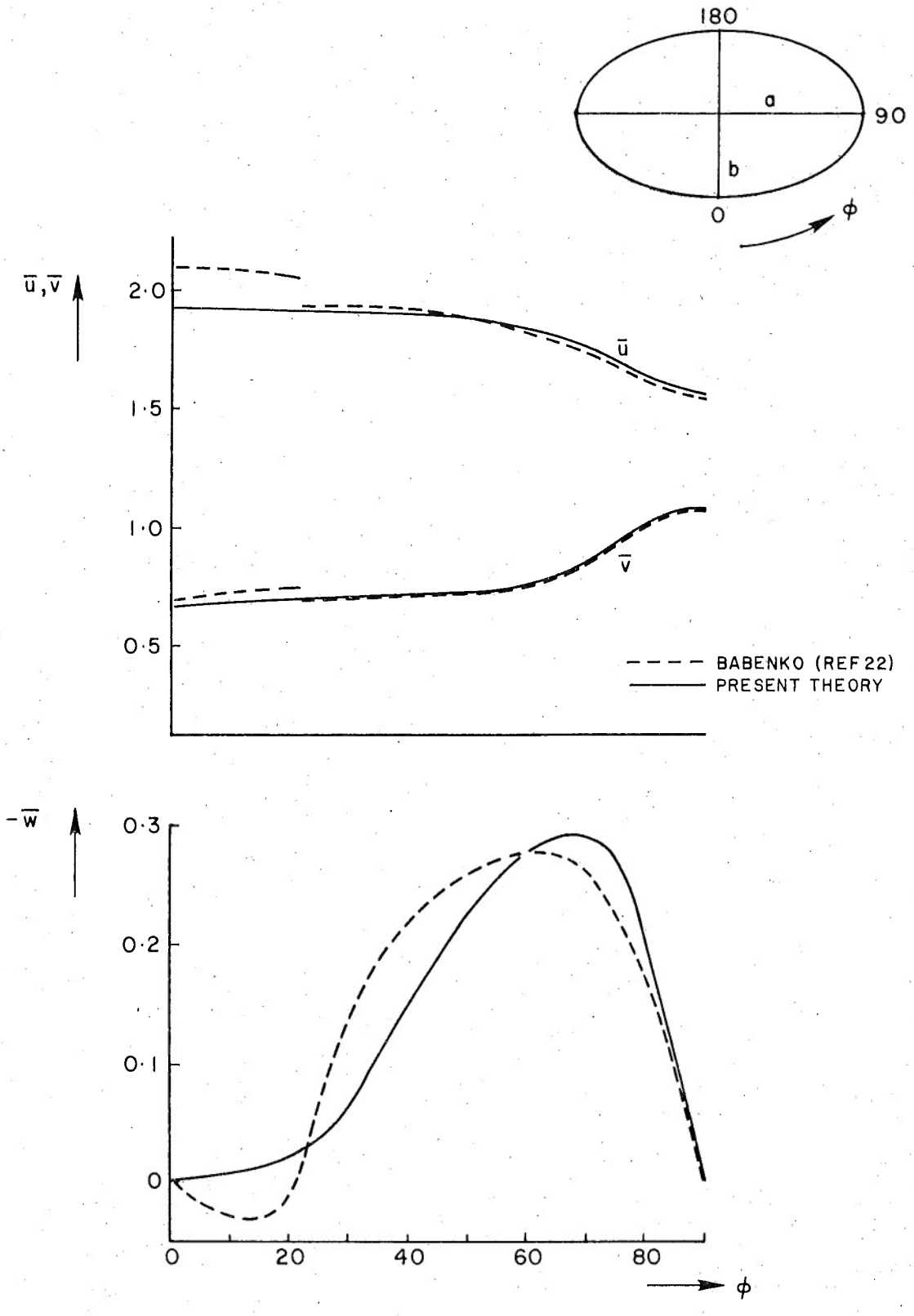

FIG. 18: ELLIPTIC CONE
SURFACE VELOCITY DISTRIBUTIONS AT ZERO INCIDENCE

$M_\infty = 10$, $a = 0{\cdot}7$, $b = 0{\cdot}35$

APPENDIX A

NUMERICAL PROCEDURE FOR SOLVING ELLIPTIC PARTIAL DIFFERENTIAL EQUATIONS

A.1.0 NOTATION

(x, y)	co-ordinate system
U	a function of (x, y)
x_0, x_1	lower and upper limits on x
y_0, y_1	lower and upper limits on y
$F(y)$	a function of y at $x = x_0$
$\epsilon\ (y)$	a function of y at $x = x_1$
ϵ_k	value of $\epsilon\ (y)$ at the kth line at $x = x_1$
F_i	value of $F(y)$ at the ith line at $x = x_0$
U_i	a value of U on the ith line
p_i	a value of p on the ith line
$f\left(U, \frac{\partial U}{\partial x}\right)$	boundary condition at $x = x_1$ is that $f\left(U, \frac{\partial U}{\partial x}\right)$ is zero.

A.2.0 METHOD

Suppose (x, y) are independent variables and U is any function of (x, y) defined by partial differential equations within a region $x_0 \leq x \leq x_1$ and $y_0 \leq y \leq y_1$. Boundary conditions for U or its normal derivatives are given on the bounds of the above region.

By estimating some unknown function (or functions) at one of the boundaries (say, for example, $\frac{\partial U}{\partial x} = F\ (y)$ at $x = x_0$, $y_0 \leq y \leq y_1$), and by replacing the derivatives in the y direction by differences, thus making the partial differential equations into ordinary differential equations, the equations can be integrated from x_0 to x_1 in a way similar to that for integrating parabolic partial differential equations. At $x = x_1$ there are given boundary conditions, of the form $f\left(U, \frac{\partial U}{\partial x}\right) = 0$, to be satisfied, but the preceding integration, assuming the estimate at $x = x_0$ is not correct, would give a residual of $f\left(U, \frac{\partial U}{\partial x}\right) = \epsilon\ (y)$, say. To solve the elliptic problem completely the estimated function at $x = x_0$ must be improved until $\epsilon\ (y)$ is sufficiently small.

To carry out the above integration (using an estimate of $\frac{\partial U}{\partial x}$ at $x = x_0$) the region is first divided into strips of width δy and first or second derivatives replaced by differences

$$\left(\frac{\partial U}{\partial y}\right)_{x,y} = \frac{U(x, y + \delta y) - U(x, y - \delta y)}{2\,\delta y} + 0\,(\delta y^2)$$

$$\left(\frac{\partial^2 U}{\partial y^2}\right)_{x,y} = \frac{U(x, y + \delta y) - 2U(x, y) + U(x, y - \delta y)}{\delta y^2} + 0\,(\delta y^2)$$

or alternatively by more accurate formulae such as

$$\left(\frac{\partial U}{\partial y}\right)_{x,y} = \frac{4}{3}\left[\frac{U(x, y + \delta y) - U(x, y - \delta y)}{2\,\delta y}\right] - \frac{1}{3}\left[\frac{U(x, y + 2\delta y) - U(x, y - 2\delta y)}{4\,\delta y}\right]$$

$$+ 0\,(\delta y^4) \qquad \text{(A-1)}$$

for a first derivative. The partial differential equations thus become a set of coupled ordinary differential equations in one independent variable x with differential equations for each of the dividing lines in the region $y_0 \leq y \leq y_1$ and with the differential coefficient at any line depending on variables to both sides of that line. These resulting ordinary differential equations can then be integrated by standard techniques, one of the most efficient being the Hamming predictor modifier corrector method (Ref. 14). This method was used in calculations presented in this Report; the starting procedure employed was the Runge Kutta method given, for example, in Reference 20.

Once an integration has been made from one boundary to the other (x_0 to x_1 in the case above) the residual function $\epsilon(y)$ is known for the given estimate $F(y)$. To improve the estimate $F(y)$ so that $|\epsilon(y)|$ is made smaller, the following method is used.

The function $F(y)$ can be defined by its values at $F(y_0 + j\delta y)$ ($j = 0, 1 \ldots n$; $y_0 + n\delta y = y_1$), and similarly $\epsilon(y)$ is represented by its values at $\epsilon(y_0 + j\delta y)$. Therefore determining a procedure to minimise $|\epsilon(y)|$ is equivalent to finding a procedure to minimise $\sum_{k=0}^{n} \epsilon^2\,(y_0 + k\delta y)$ with respect to $F\,(y_0 + j\delta y)$, $j = 0, 1 \ldots n$. Many methods exist for minimisation; one of the best for minimising a sum of squares is presented by Powell (Ref. 21). This method is similar to the generalized least squares technique given by the iterative process

$$\sum_{j=0}^{m} \left\{ \sum_{k=0}^{n} \frac{\partial \epsilon_k}{\partial F_i} \frac{\partial \epsilon_k}{\partial F_j} \right\} \delta F_j = - \sum_{k=0}^{n} \epsilon_k \frac{\partial \epsilon_k}{\partial F_i} \qquad (i = 0, 1 \ldots m) \qquad \text{(A-2)}$$

where, in the above case, the number of unknowns m is equal to n. $\epsilon_k \equiv \epsilon\,(y_0 + k\delta y)$ and

$F_i \equiv F(y_0 + i\delta y)$ and δF_j is the improvement to be made to F_j so that $\sum_{k=0}^{n} \epsilon_k^2$ is minimised.

In the generalised least squares technique "steps" defined by (A-2) are made until either $\sum \epsilon_k^2$ or $\delta F_j/F_j$ is sufficiently small. Each step requires calculating $\partial\epsilon_k/\partial F_i$ by differences

$$\frac{\partial \epsilon_k}{\partial F_i} \approx \frac{\epsilon_k (F_0, F_1 \ldots, F_i + \triangle F_i, \ldots F_m) - \epsilon_k (F_0, F_1 \ldots F_i \ldots F_m)}{\triangle F_i} \qquad \text{(A-3)}$$

for $i = 0, 1, 2 \ldots m$,

where ϵ_k is considered as a function of $F_0, F_1 \ldots F_m$ since, for given values of $F_0, F_1 \ldots F_m$, the corresponding values of ϵ_k ($k = 0, 1 \ldots n$) can be found by integration as described previously. $\triangle F_i$ is a small increment in F_i, say $10^{-6} F_i$ if $F_i \neq 0$. Now in Powell's method only the first "step" requires the use of (A-3), and after the first step the partial derivatives can be calculated from values of ϵ_k ($k = 0, 1 \ldots n$) already obtained on the previous step. Thus Powell's method is more efficient than the generalised least squares technique and it is also claimed to ensure convergence.

It should be noted that it is not necessary to define the function $F(y)$ by its values at $y_0 + j\delta y$ ($j = 0, 1 \ldots n$). In fact it is more economical to define $F(y)$ by as few "unknowns" as possible in order to reduce the computation required for the first step given by (A-3). For instance, the first few terms of a Fourier series expansion could be used if it is known that $F(y)$ can be adequately represented in this way, which is the case for a circular cone at incidence and for the other conical bodies discussed in this Report.

A simple example illustrates the above method. To solve

$$\frac{\partial^2 U}{\partial x^2} + \frac{\partial^2 U}{\partial y^2} + 1 = 0 \qquad \text{(A-4)}$$

given $U = 0$ on $x = 0, 1$ and on $y = 0, 1$. From symmetry it is sufficient to solve the problem for the region $0 \leq x \leq \frac{1}{2}$, $0 \leq y \leq \frac{1}{2}$ with boundary conditions

$$U = 0 \quad \text{on } x = 0 \text{ and on } y = 0$$

$$\frac{\partial U}{\partial x} = 0 \text{ on } x = \tfrac{1}{2} \text{ and } \frac{\partial U}{\partial y} = 0 \text{ on } y = \tfrac{1}{2}$$

Divide the region $0 \leq x \leq \frac{1}{2}, 0 \leq y \leq \frac{1}{2}$ into strips as shown, and number the lines forming the strips 0, 1, 2, ... n

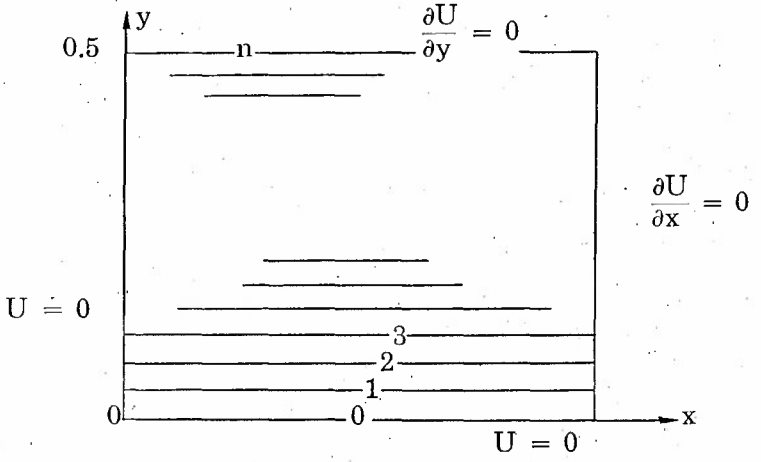

Replace $\frac{\partial^2 U}{\partial y^2}$ at line i by the difference approximation

$$\frac{U_{i+1} - 2U_i + U_{i-1}}{\delta y^2}$$

Let $p_i = \left(\frac{\partial U}{\partial x}\right)_i$, then equation (A-4) can be written

$$\left.\begin{aligned} &\frac{dp_i}{dx} + \frac{U_{i+1} - 2U_i + U_{i-1}}{\delta y^2} + 1 = 0 \\ \text{also} \quad &\frac{dU_i}{dx} = p_i \end{aligned}\right\} \qquad \text{(A-5)}$$

Now the set (A-5) represents a set of ordinary differential equations. The boundary condition $\frac{\partial U}{\partial y} = 0$ on $y = 0.5$ can be satisfied by the difference approximation $U_{n+1} = U_{n-1}$. The equations (A-5) are subject to boundary conditions at $x = 0$

$$U_i = 0$$

$$p_i = F(y_i)$$

On estimating F(y), the set (A-5) can be integrated to $x = 0.5$ giving residual errors $\epsilon(i\delta y) = p_i$ at $x = 0.5$ (we require $p_i = \frac{dU_i}{dx} = 0$ at $x = 0.5$). One can then make small displacements to F(y) as in (A-3) and use (A-2) to improve the estimate of F(y).

An advantage of the above procedure is that if the differential equations and boundary conditions are linear as in the above example, then the correct solution will be obtained after only one step given by (A-2), since in this case the ϵ_k are linear functions of F_i. A disadvantage of such an approach is that reasonably good initial estimates of F_i may be necessary in order that the integration will not diverge.

APPENDIX B

A METHOD FOR SOLVING THE SURFACE EQUATIONS FOR THE CIRCULAR CONE AT INCIDENCE

The surface pressure is given by the method of Section 3.0, but it is necessary to calculate u, v, w, and ρ from equations (6), (11), (12), and (13). Obviously the density follows directly from equation (11) where the constant in that equation is the value of $\left(\frac{p}{\rho^{\gamma}}\right)$ at $\phi = 0$.

At the windward and leeward axes ($\phi = 0, \pi$), $w = 0$ from the symmetry of the problem, hence at these two points u and v can be calculated from (6) and (12). Equation (13) $u_{\phi} + Gv_{\phi} = wG$ is replaced by differences as in equation (A-1). These difference equations are written at every point where p is given (except at 0, π) and, together with (6) and (12) written at every such point, give a set of non-linear algebraic equations. These equations can then be solved by usual techniques. The method employed here was that of Reference 21, since this method is efficient and was already being used to solve the main part of the problem.

APPENDIX C

THE POSITION OF NODAL AND SADDLE TYPE SINGULAR POINTS

It has been noted in Reference 7 that singular points will always exist in conical flow without axial symmetry. We define a nodal type singular point as a point where surface streamlines converge and a saddle type singular point as one where the surface streamlines diverge. At a nodal type singular point, discontinuities in entropy will exist giving a discontinuity in some other quantities, while at the saddle type singular point no discontinuities will exist. In this Section we will consider the position of the singular points for a circular cone at incidence and also for an elliptic cone at zero incidence.

The position of a singularity is important since, if it should move off the surface, it is not possible to integrate the equations (5) past this singularity. On the other hand, a knowledge of their position on the surface is also important, since this would affect the solution of the surface equations (6), (11), (12), (13).

We know that a singular point is defined by the two conditions

$$w = 0 \tag{C-1a}$$

and the main diagonal of matrix B should be zero, that is

$$\xi_z u + \xi_r v + \frac{\xi_\theta}{r} w = 0 \tag{C-1b}$$

since equations (9d) and (9e) can be combined to give $\left(\xi_z u + \xi_r v + \frac{\xi_\theta}{r} w\right) \frac{\partial S}{\partial \xi} + \frac{w}{r} \frac{\partial S}{\partial \phi} = 0$ where $S = \log \frac{p}{\rho^\gamma}$ and, hence, when conditions (C-1) are satisfied S is indeterminate.

Now (C-1b) is satisfied at the surface as a boundary condition, and because of the symmetry about $\phi = 0$ and π in the case of a circular or elliptic cone, we also know that $w = 0$ at $\phi = 0$ or π (as well as at $\phi = \pi/2$ for the elliptic cone at zero incidence). Thus a singular point is always present at a point on the body and in a plane of symmetry for the conditions being considered.

C.1.0 THE CIRCULAR CONE AT INCIDENCE

It is shown in Reference 9 that for the circular cone at incidence a saddle type singular point is present at the windward generator $\phi = 0$ and that a nodal type singular point is present at the leeward generator $\phi = \pi$ until the surface pressure becomes adverse. It is then shown that this nodal singularity may move away from the leeward generator to follow the point of minimum circumferential pressure, or that it may stay at the leeward generator until a certain critical incidence is reached, when it would lift off the surface. The following analysis shows that the latter situation is, in fact, what happens to this nodal singularity.

To determine whether the nodal singularity can move along the leeward plane of symmetry and off the surface, we consider the quantity $[\xi_z u + \xi_r v]_{\xi = 1, \phi = \pi}$ which, as the normal component of the velocity at the shock, must be negative in the sign convention being used. We also consider

$$\left[\frac{\partial}{\partial \xi}\left(\xi_z u + \xi_r v\right)\right]_{\xi = 0, \phi = \pi}$$

and show that this derivative becomes positive under the conditions given in Reference 9 for the singularity to move away from $\xi = 0, \phi = \pi$. Thus, since $\xi_z u + \xi_r v = 0$ at $\xi = 0$ (the normal velocity), it follows that $\xi_z u + \xi_r v$ will pass through another zero along the leeward plane of symmetry as well as being zero on the surface.

It will also be shown that the nodal singularity will not move along the surface away from the leeward generator. Thus, the nodal singularity will move into the flow field along the leeward plane of symmetry.

C.1.1 To Show That $\left[\frac{\partial}{\partial\xi}\left(\xi_z u + \xi_r v\right)\right]_{\xi = 0,\ \phi = \pi}$ Becomes Positive At A Certain Critical Incidence

Consider equation (9c), which applies at the surface $\xi = 0$

$$-\frac{\xi_r G_\phi}{\rho G} p_\xi + \frac{w}{G} w_\phi + \frac{p_\phi}{\rho G} = -\frac{w v}{G}$$

since $d = 0$ is a surface boundary condition. Now differentiate this equation with respect to ϕ and consider the result at a plane of symmetry ($G_\phi = w = p_\phi = 0$) giving

$$-\frac{\xi_r G_{\phi\phi}}{\rho} p_\xi + w_\phi^2 + \frac{p_{\phi\phi}}{\rho} + w_\phi v = 0$$

or

$$w_\phi = \tfrac{1}{2}\left[-v \pm \sqrt{v^2 - 4\left(\frac{p_{\phi\phi}}{\rho} - T\right)}\right] \tag{C-2}$$

where $T = \xi_r G_{\phi\phi} p_\xi/\rho$ and must be zero, since from (9b) it follows that if $w = 0$ then $p_\xi = 0$. For the circular cone, in the leeward or windward plane of symmetry the positive sign obviously applies at incidence $\alpha = 0$, since we then know that $p_{\phi\phi} = w_\phi = 0$ and it seems from the results obtained, using the method of this Report or from those of Reference 11, that the + sign always applies on the windward side. The + sign applies also on the leeward side until an incidence is reached where $v^2 = 4\, p_{\phi\phi}/\rho$, when the sign changes to −, and this seems to occur at relative incidences α/θ_c between 0.2 (for slender bodies) and about 0.4 (for hypersonic conditions).

Now consider equation (9d′) at the plane of symmetry and at the cone surface

$$\frac{\partial}{\partial\xi}\left[\xi_z u + \xi_r v\right] = -\left[u + \frac{v + w_\phi}{G}\right]$$

and substitute for w_ϕ from (C-2)

$$\frac{\partial}{\partial\xi}\left[\xi_z u + \xi_r v\right] = \frac{1}{2G}\left[\mp\sqrt{v^2 - 4p_{\phi\phi}/\rho} - v - 2uG\right] \tag{C-3}$$

Now u and v are always positive on the cone surface in the sign convention used, hence, when the + sign in (C-2) applies, it follows that $\frac{\partial}{\partial\xi}(\xi_z u + \xi_r v) < 0$ and the singularity stays on the surface. When the − sign in (C-2) applies, $\frac{\partial}{\partial\xi}(\xi_z u + \xi_r v)$ is still negative until an incidence is reached such that

$$\sqrt{v^2 - 4\, p_{\phi\phi}/\rho} > v + 2uG$$
$$= 3v$$

since on the surface at the plane of symmetry from (6) we have $v = uG$. Alternatively, this condition can be written

$$p_{\phi\phi} < -2\rho v^2$$

or in terms of surface Mach number M_c, surface pressure p_c and cone semi-angle θ_c

$$p_{\phi\phi} < -2\gamma\, p_c\, M_c^2 \sin^2 \theta_c$$

This is the expression formed in Reference 9 for the singularity to move away from $\xi = 0$, $\phi = \pi$.

C.1.2 To Show That the Singularities Cannot Move from the Planes of Symmetry.

When the singularity does move, and, in fact, for incidences above that incidence when the sign in (C-2) first changes (i.e. $v^2 = 4p_{\phi\phi}/\rho$ at the leeward generator), which always occurs before adverse pressure starts, we know that the $-$ sign applies in the expression (C-2) for w_ϕ at the leeward plane, that is

$$w_\phi = \tfrac{1}{2}\left[-v - \sqrt{v^2 - 4p_{\phi\phi}/\rho}\ \right]$$

which is always negative. On the other hand, at the windward plane we have

$$w_\phi = \tfrac{1}{2}\left[-v + \sqrt{v^2 - 4p_{\phi\phi}/\rho}\ \right]$$

and it is observed from results that a pressure maximum always exists at $\phi = 0$, so that $p_{\phi\phi} < 0$, thus $w_\phi > 0$. Hence, it is shown that at the surface $w_\phi > 0$ on the windward plane and $w_\phi < 0$ on the leeward plane, and since w is zero at $\phi = 0$ and π, other zeros in w could only occur on the surface if they were to occur in pairs. Now a zero in w can only occur at a surface pressure minimum or maximum, and apart from the minimum and maximum pressure at the windward and leeward generators, it is observed from results that only one other minimum occurs at incidences greater than that at which adverse pressure first starts. Hence w cannot be zero except at the windward and leeward generators.

Thus the singularity situation for a circular cone at incidence is as follows. A saddle type singularity is always situated at the windward generator and a nodal singularity is at the leeward generator until an incidence is reached when $p_{\phi\phi} < -2\gamma\, p_c\, M_c^2 \sin^2 \theta_c$. For incidences above this, the nodal singularity will be situated off the surface along the leeward plane of symmetry.

These conclusions on the position of the singularity are, in fact, verified by results obtained in certain cases for the circular cone at incidence, and a plot of $\frac{r}{\xi_r}(\xi_z u + \xi_r v)$ and $\frac{\partial}{\partial \xi}\left[\frac{r}{\xi_r}(\xi_z u + \xi_r v)\right]$ against ξ along $\phi = \pi$ is given in Figure 15 for the case $M_\infty = 1.797$, $\theta_c = 12.5°$. Figure 16 shows a plot of $\bar{p}_{\phi\phi} + 2\bar{\rho}\,\bar{v}^2$ at the leeward generator against relative incidence α/θ_c for the same case.

It should be noted that it is possible by the present method to obtain solutions for some cases where the singularity moves off the surface, since extrapolation of $\xi_z u + \xi_r v + \frac{\xi_\theta w}{r}$ from $\xi = \delta\xi$ to $\xi = 0$, as described in Section 3.0, is made. It also appears to be valid to extrapolate pressure through this singularity. The singularity does not cause trouble until it moves so far out that it

is at a distance corresponding to ξ approaching $\delta\xi$ from the surface, so that results can still be obtained for moderately large relative incidences (assuming that $\xi_z u + \xi_r v$ and p are continuous through these singularities).

C.2.0 ELLIPTIC CONE AT ZERO INCIDENCE

Since the elliptic cone at zero incidence is symmetric about $\phi = 0$ and $\phi = \pi/2$, only the section $0 \leq \phi \leq \pi/2$ of the flow field needs to be considered.

Consider the pressure distributions around elliptic cones in the section $0 \leq \phi \leq \pi/2$. They have the forms shown, for example, in Figure 17, which shows the form variation against various values of a/b where a is the semi-major axis and b is the semi-minor axis. The minor axis lies in the plane $\phi = 0, \pi$. From these distributions it can be seen that the pressure is monotonic except in the cases a/b = 2.4 and 2.8. It is the opinion of the author that the non-monotonic behaviour in these latter cases is due to "numerical overshoot" of the pressure, since the numerical procedure is trying to fit an almost constant pressure in the region $0 \leq \phi \leq 40°$ followed by a rapidly varying pressure in the region $40° \leq \phi \leq 90°$ — in fact, in the author's opinion, the pressure will always be monotonic for all a/b whatever the free stream Mach number.

On the assumption that the pressure is monotonic in the region $0 \leq \phi \leq \pi/2$, it is easily seen that w cannot be zero except at $\phi = 0, \pi/2$ as follows. If $w = 0$ on the surface, then from equation (9b) we must have $\frac{\partial p}{\partial \xi} = 0$, and hence from equation (9c) a necessary condition for w to be zero is that $\frac{\partial p}{\partial \phi}$ must be zero. However, for the elliptic cone at zero incidence, since p is monotonic, w can only be zero at $\phi = 0, \pi/2$.

The above analysis contradicts Reference 22, where results are given that show that for $M_\infty = 10$, a = 0.7 and a/b = 2, a nodal type singularity existed on the cone surface at about $\phi = 20°$ with saddle type singularities at $\phi = 0$ and $\pi/2$. Plots of some results for this same case, using the present method, are given in Figure 18. They indicate a nodal type singularity at $\phi = 0$ with a saddle type singularity at $\phi = \pi/2$.

It still must be determined whether the singularities can move off the surface for the elliptic cone at zero incidence. It can be shown that for the elliptic cone the formulae for w_ϕ and $\frac{\partial}{\partial \xi}(\xi_z u + \xi_r v)$ given by (C-2) and (C-3) apply at the planes of symmetry at the cone surface, but the appropriate signs have to be determined. Clearly when a/b = 1, $p_{\phi\phi} = w_\phi = 0$ everywhere and, hence, the + sign holds in (C-2) and the − sign in (C-3). Now if we assume a sign change takes place continuously in w_ϕ as a/b increases, this would imply that $v^2 - 4p_{\phi\phi}/\rho = 0$ would be a necessary condition for the change, but at $\phi = \pi/2$ it is observed that $p_{\phi\phi} < 0$ always for a/b > 1, hence $v^2 - 4p_{\phi\phi}/\rho$ is never zero, implying that the − sign is always applicable in equation (C-3). This in turn implies that $\frac{\partial}{\partial \xi}\left[\xi_z u + \xi_r v\right]_{\xi = 0,\ \phi = \pi/2}$ is always negative. Also, since $\left[\xi_z u + \xi_r v\right]_{\pi/2}$ is zero on the cone surface and is negative at the shock, it follows that this singularity stays on the surface. On the other hand, at $\phi = 0$, since $p_{\phi\phi} > 0$ always for a/b > 1, then clearly whichever sign applies in equation (C-3) it follows that $\left[\frac{\partial}{\partial \xi}(\xi_z u + \xi_r v)\right]_{\xi = 0,\ \phi = 0} < 0$, and by the same argument as above, the singularity stays on the surface.

Thus, in conclusion, the singularities stay at the cone generators in the planes of symmetry for the elliptic cone at zero incidence.

APPENDIX D

THE SOLUTION FOR A CIRCULAR CONE AT ZERO INCIDENCE

The computations to generate the zero order solution are straightforward once a reasonable initial estimate of the shock angle is determined. The method will be described without going into mathematical details.

An estimate of the shock angle is made empirically from results obtained by Sims (Ref. 2) for situations involving conically slender bodies ($M_\infty \sin \theta_c \leq 0.6$) and from hypersonic small disturbance theory for $M_\infty \sin \theta_c > 0.6$. These estimates then take the form

$$M_\infty \sin \theta_s - 1 = \frac{\gamma + 1}{2} (M_\infty \sin \theta_c)^{3.63} \qquad \text{for } M_\infty \sin \theta_c \leq 0.6$$

and

$$\frac{\sin \theta_s}{\sin \theta_c} = \left[\frac{\gamma + 1}{2} + \frac{1}{M_\infty^2 \sin^2 \theta_c} \right]^{\frac{1}{2}} \qquad \text{for } M_\infty \sin \theta_c > 0.6$$

where θ_s is the shock wave angle.

Having obtained these estimates of the shock angle, quantities behind the shock can be determined and the equations of motion integrated into the body, thus giving a residual normal velocity on the surface. An iteration procedure due to Wegstein (Ref. 23) is then used to improve the estimate of the shock angle so that the residual normal velocity is made very close to its required value of zero. It is found that this computation requires only three or four iterations, hence only a few seconds of computer time.

APPENDIX E

SOME COMMENTS ON THE COMPUTER PROGRAM

E.1.0 THE INCLUSION OF FURTHER FOURIER COEFFICIENTS TO REPRESENT THE SHOCK SHAPE

As the incidence or other perturbation is increased, the number of Fourier coefficients in the shock wave equation $F(\phi) = \sum_{i=0}^{m} F_i \cos i\phi$ must be increased. At each incidence the estimated F_m (i.e. the last coefficient) is compared with $\sum_{i=0}^{m} F_i$ (the tangent of the shock angle at $\phi = 0$), and if $|F_m| \Big/ \sum_{i=0}^{m} F_i > 5 \times 10^{-5}$, an extra coefficient is added so that the shock wave equation is now $F(\phi) = \sum_{i=0}^{m+1} F_i \cos i\phi$ where $F_0, F_1 \ldots\ldots F_m$ have the same values as were estimated previously and the estimate for F_{m+1} is zero. An extra coffiecient is also added if the sum of squares of residuals on the preceding calculation is greater than 2×10^{-6}.

E.2.0 STEP LENGTHS

Step lengths of $22\frac{1}{2}°$ and 0.1 in ϕ and ξ respectively seem to give sufficiently accurate results for all the cases computed so far for the circular cone at incidence. To keep the step length of $22\frac{1}{2}°$ in ϕ implies that no more than nine Fourier coefficients can be used to represent the shock shape, since the number of unknowns defining the shock must not exceed the number of dividing lines in the region $0 \leq \phi \leq \pi/2$. Thus, when the criterion in Section E-1.0 is satisfied to include a tenth coefficient, the Fourier series representation to the shock is not used; instead the shock is simply represented by values at discrete points $\phi = 0, 22\frac{1}{2} \ldots\ldots 180°$. Initial estimates at these discrete points are found by extrapolation as before. The iteration procedure then improves these estimates at the discrete points.

In the cases of the elliptic cones and the fourth order cosine Fourier series body, the increment in ϕ is taken as 22.5° to start with, i.e., when the configuration is near to a circular cone at zero incidence (this is equivalent to 8 sections and 9 lines in the range $0 \leq \phi \leq 180°$). As the incidence or eccentricity or other perturbation increases, further Fourier coefficients are added to the sum forming the shock $r = F(\phi)$, and when the number of coefficients is about to exceed the number of dividing lines in the region $0 \leq \phi \leq 180$, the number of lines is increased so that their number is always equal to the number of coefficients. It is necessary to do this in order that the number of discrete normal velocities at the surface is not less than number of unknowns defining the shock, which is a necessary condition for the iteration process.

E.3.0 EXTRAPOLATION TO THE BODY

Integration was always made to a value $\xi = 0.1$ in equal steps $\delta\xi$. The velocity $\xi_z\, u + \xi_r\, v + \frac{\xi_\theta}{r} w$ was then extrapolated, using the values and derivatives of this quantity at 0.1, $0.1 + \delta\xi$, $0.1 + 2\,\delta\xi$, and $0.1 + 3\,\delta\xi$, by solving the formulae

$$q(0) = q\,(\delta h) - \delta h\, q'\,(\delta h) + \frac{\delta h^2}{2}\left[q''(0) + \delta h\, q'''(0) + \frac{\delta h^2}{2}\, q^{iv}(0) \right]$$

$$- \frac{\delta h^3}{6}\left[q'''(0) + \delta h\, q^{iv}(0) \right] + \frac{\delta h^4}{24}\, q^{iv}(0) + 0\,(\delta h^5)$$

where $\delta h = 0.1 - (j - 1)\,\delta\xi \quad \text{for } j = 1, 2, 3, 4 \;(\delta\xi < 0)$

and q represents the quantity to be extrapolated.

When the iteration procedure is completed the differential equations are integrated to a value ξ of approximately 0.003 and the pressure is then extrapolated to the surface by a quadratic formula.

E.4.0 COMPUTING TIMES

Typical times on an IBM 360/50 computer for the circular cone at one incidence are 40 seconds to 1 minute for relative incidences up to 0.6; times for higher relative incidences vary from 1 to 3 minutes approximately. Actual times are given below for certain typical cases.

E.4.1 Circular Cone

$M_\infty = 7$ $\theta_c = 25°$

$\frac{\alpha}{\theta_c}$	Time (min.)
0.01	0.7
0.1	0.6
0.2	0.6
0.3	0.7
0.4	0.7
0.5	0.8
0.6	1.0
0.7	1.2

$M_\infty = 1.797$ $\theta_c = 12.5°$

$\frac{\alpha}{\theta_c}$	Time (min.)
0.01	0.7
0.1	0.6
0.2	0.8
0.3	0 7
0.4	0.7
0.5	0.7
0.6	0.7
0.7	0.9
0.8	0.9
0.9	1.0
1.0	1.1
1.1	1.1
1.2	1.1
1.3	1.1
1.4	2.5

E.4.2 Elliptic Cone

$M_\infty = 10$ $\quad a = 0.7$ $\quad \alpha = 0$

a/b	Time (min.)
1.01	0.5
1.2	0.5
1.4	0.6
1.6	0.8
1.8	1.3
2.0	1.8
2.2	2.7
2.4	4.3
2.6	5.7
2.8	10.0

$M_\infty = 2$ $\quad a = 0.2217$ $\quad b = 0.18475$

$\frac{\alpha^\circ}{10}$	Time (min.)
0.01	1.2
0.1	1.1
0.2	1.0
0.3	1.0
0.4	1.2
0.5	1.2
0.6	1.2
0.7	1.3
0.8	1.3
0.9	1.3
1.0	1.4
1.1	1.5
1.2	2.9
1.3	4.1

E.5.0 TERMINATION OF THE ITERATION PROCEDURE

The iteration procedure is continued until the change in each Fourier coefficient is less than 10^{-6} of that Fourier coefficient. An alternative criterion for terminating the iteration is also used; this is based on the sum of squares of residual errors being less than 10^{-6}. It was found that for small relative incidences up to about 0.6, only one step in the iteration procedure was required to give sufficient accuracy. This one step requires about 10 to 15 integrations of the equations from the shock to the body. For higher relative incidences about 2 to 4 steps were necessary, requiring about 15 to 30 integrations of the equations.

E.6.0 PROGRAM AVAILABILITY

Duplicate program decks are available upon application to the High Speed Aerodynamics Section, National Aeronautical Establishment.

A description of the program and its use is given in Reference 24.